*J. Fluid Mech.* (1981), *vol.* 110, *pp.* 381–410
*Printed in Great Britain*



# Some effects of surface tension on steep water waves. Part 3

By S. J. HOGAN

Department of Applied Mathematics and Theoretical Physics,
University of Cambridge, Silver Street, Cambridge CB3 9EW

(Received 4 June 1980 and in revised form 20 January 1981)

This is the final part in the work on steady gravity–capillary waves by the author. On extending the work of Pierson & Fife (1961), the phenomenon of Wilton's ripples is resolved. These singularities of the traditional solution procedure are merely consequences of the non-uniformity in the ordering of the Fourier coefficients of the wave profile. Results presented here include wave properties and profiles. Near-resonant waves are also considered. Good agreement is found between this work and previous papers in the series as well as with other authors. An appendix contains all the results in numerical form. Minor algebraic errors in Wilton's original work are corrected.

## 1. Introduction

In recent work of the present author (Hogan 1979*a*, 1980*a*, referred to as I and II respectively) results were given for wave properties throughout most of the gravity–capillary wave range. Full details of the problem are given in those papers. I contained exact relationships between integral properties which are valid for all waves, as well as giving exact expressions for these properties in the special case of pure capillary waves (gravitational effects absent). The work of Schwartz (1974) was extended in II to include the surface tension. Capillary waves (wavelength less than 2 cm in water) were found to be similar in many respects to pure capillary waves. Gravity waves (more than 20 cm long) were similar to pure gravity waves, that is, when surface tension effects are absent.

An unexpected result for capillary waves was the rapid decrease with increasing wave height of the gravitational potential energy, $V_g$ (see equation II(3.12) for definition). This decrease, after the expected increase, is intimately connected with the extreme distortion of the profile (and hence dramatic rise in surface potential energy $V_\tau$) as the wave gets higher and starts to enclose a bubble of air in its trough. As a result the crest height of the wave above the mean level is not a monotonic function of the wave height. This was shown, analytically, to be true also for pure capillary waves (see I for details). For gravity waves it was found that the type of non-monotonicity associated with integral properties of pure gravity waves disappeared with increasing relative importance of surface tension to gravity. A measure of this importance is given by the dimensionless parameter $\kappa$ defined as

$$\kappa = 4\pi^2\tau/\lambda^2 g, \tag{1.1}$$

where $\tau$ is the surface tension coefficient divided by the density, $\lambda$ is the wavelength

and $g$ is the acceleration due to gravity. Schwartz's solution procedure failed at the so-called Wilton's (1915) ripples corresponding to values of $\kappa = 1/n$ ($n = 2, 3, \ldots$).

By a remarkable coincidence three separate independent pieces of work, on the same subject, were completed at around the same time as I and II. It is not the purpose of this paper to compare the four different approaches. Rather we summarize very briefly each method and some of their principal results. Rottman & Olfe (1979) derived an integral equation for the wave profile $y = \eta(x)$, using an image flow. Despite the fact that they did not parametrize the $(x, y)$ co-ordinates, thus excluding profiles multivalued in $y$, they obtained numerical results for wave properties of pure capillary waves with no vertical tangents and wave profiles of waves at and near $\kappa = \frac{1}{2}$. They noted that, for a given value of $\kappa$, a full wave profile of certain height was identical with a half-wave profile with a parameter value $4\kappa$. Schwartz & Vanden-Broeck (1979) used a more powerful technique, centred on the Hilbert formulae for the unit circle. This involves the Cauchy principal part of an integral. They took $r$ points on the wave profile and, with the phase speed $c$, solved the resulting $r+1$ equations by Newton's method. They found no singular behaviour at $\kappa = 1/n$. They also found several solutions for a given $\kappa$ by means of simple numerical analytic methods.

A complete explanation of Wilton's ripples is given by Chen & Saffman (1979, 1980). They generalized Wilton's approach by not restricting attention to one wavelength. In the same sense that Wilton's ripples can be regarded as the result of a wave of length $L$ interacting with another length $L/N$ ($N \geqslant 2$), Chen & Saffman have shown that other interactions are possible, with waves of length $ML/N$ ($M$, $N$ coprime and $M > N \geqslant 1$ without loss of generality). They solved an integral equation for the wave profile as well as using a Fourier decomposition approach. They adopted a terminology for linear waves which we will use here. Waves with leading Fourier coefficient $a_N$ ($N \geqslant 1$) are said to be 'of degree $N$'. It is assumed that no other coefficient is of the same or lower order. In fact, $a_n = O(a_N^{n/N})$ for $n = pN$, where $p$ is a positive integer and $a_n \equiv 0$ otherwise for these waves. Waves with coefficients $a_N$ and $a_M$ of the same order are called 'combination $(M, N)$' waves. Stokes' waves are waves of degree 1 and Wilton's ripples are combination $(M, 1)$ waves. This is not exactly the same terminology as given by Chen and Saffman, who refer to pure waves of a certain degree. But the adjective pure has been used to describe waves whose propagation is governed by only gravity or capillary effects (as opposed to both effects at the same time).

Following the known failure of the Stokes expansion at the Wilton ripples (as improved by Schwartz), a modified version is offered here as an extension to the procedure of Pierson & Fife (1961). We concentrate on the combination (2, 1) waves at $\kappa = \frac{1}{2}$, although the method can be extended to include other waves at other singularities. In addition near-singular waves are also considered. We attempt to explore the regions unreached by the series expansion methods of II, where convergence was non-existent, for example, at $\kappa = 0{\cdot}6$ and the wave semi-height, $h \geqslant 0{\cdot}3$. We are therefore only considering a particular branch of the solutions.

It should be noted that the work of II on gravity–capillary waves does not contradict the conclusion of Chen & Saffman that the limit $\kappa \to 0$ is singular for waves of a given degree. They do not show that a combination wave (or its finite-amplitude equivalent) is incapable of being continued to a pure gravity wave. We cannot,

however, completely exclude from our results the possibility of limit line behaviour, which may show up when coefficients of very high order are calculated.

In what follows, knowledge of I and II is assumed. Section 2 contains an outline of the form of the perturbation solution to be used, as well as the set of recursive equations obtained from Bernoulli's equation. The expansions for the Fourier coefficients are then given as well as for wave properties both at and near $\kappa = \frac{1}{2}$. The expansion for the pure waves of degree 2 at $\kappa = \frac{1}{2}$ are also given. In §3, we present results for wave profiles and properties of exact resonance and near-resonance combination (2, 1) waves. The breakdown of the Stokes ordering of the Fourier coefficients, *viz.* $a_n = O(a_1^n)$, is graphically illustrated. This confirms the fact that Wilton's ripples are only singular because of an assumption of the mathematics rather than some physical reason. The 'physical' explanation of resonance offered by Pierson and Fife is therefore only a guide to the deeper problem. We also show the limits of the use of Padé approximants and the extent of agreement with I and II.

A complete historical introduction to other works in this field is given in Hogan (1979*b*).

## 2. Method of solution

A method is presented for analysing waves with $\kappa$ equal and very nearly equal to $\frac{1}{2}$. Good agreement is found with the work of II and with other methods. Integral properties are also discussed.

### (*a*) *The form of the perturbation*

Wilton's re-examination of his own approximation procedure led him to the conclusion that, at $\kappa = \frac{1}{2}$, the leading Fourier coefficient was no longer the only term of its given order. In fact, the second coefficient was now of *equal* order. He also showed that each successive pair of coefficients was of equal order and of order only *one* less than the previous pair. So instead of

$$a_1 = O(\epsilon), \quad a_2 = O(\epsilon^2), \quad a_3 = O(\epsilon^3), \quad a_4 = O(\epsilon^4), \quad \ldots,$$

he found that

$$a_1 = O(\epsilon), \quad a_2 = O(\epsilon), \quad a_3 = O(\epsilon^2), \quad a_4 = O(\epsilon^2), \quad a_5 = O(\epsilon^3), \quad a_6 = O(\epsilon^3), \quad \ldots,$$

was a consistent ordering scheme. At the other singular values of $\kappa$, he advocated still further ways of ordering the coefficients. With this rearrangement in mind for the case $\kappa = \frac{1}{2}$, we now propose a general expansion for the $a_n$ which reduces to that of Wilton. Define a mapping from $\mathbb{R}$ to $\mathbb{Z}^+$, int: $a \to n$ (so $a$ is real and $n$ integral) by $n =$ the integral part of $a$, e.g. int $(\pi) = 3$, then let

$$a_i = \sum_{j=1}^{\infty} \hat{\alpha}_{ij} \epsilon^{[j-1+\text{int}(\frac{1}{2}(i+1))]} \quad (i = 1, 2, \ldots), \tag{2.1}$$

where $\epsilon$ is a suitable expansion parameter. Immediately we note that $a_i = O(\epsilon^{\text{int}(\frac{1}{2}(i+1))})$, as obtained by Wilton. Now, it is clear that none of §2 of II is changed by assuming $\kappa = \frac{1}{2}$ and so we can use all the given equations of that section without any change.

We must adopt different expansions for the $f_i$, $q_i$, $u_i$, $w_i$, $c^2$ and $K$, along similar lines to (2.1). In fact we assume

$$f_i = \sum_{j=1}^{\infty} \hat{\beta}_{ij} \epsilon^{[j-1+\mathrm{int}(\frac{1}{2}(i+1))]} \quad (i = 1, 2, \ldots), \tag{2.2}$$

$$q_i = \sum_{j=1}^{\infty} \hat{\mu}_{ij} \epsilon^{[j-1+\mathrm{int}(\frac{1}{2}(i+1))]} \quad (i = 1, 2, \ldots), \tag{2.3}$$

$$u_i = \sum_{j=1}^{\infty} \hat{\tau}_{ij} \epsilon^{[j-1+\mathrm{int}(\frac{1}{2}(i+1))]} \quad (i = 1, 2, \ldots), \tag{2.4}$$

$$w_i = \sum_{j=1}^{\infty} \hat{\zeta}_{ij} \epsilon^{[j-1+\mathrm{int}(\frac{1}{2}(i+1))]} \quad (i = 1, 2, \ldots), \tag{2.5}$$

$$c^2 = \sum_{j=0}^{\infty} \hat{\gamma}_j \epsilon^j, \tag{2.6}$$

$$K = \sum_{j=0}^{\infty} \hat{\delta}_j \epsilon^j. \tag{2.7}$$

For $\kappa = \frac{1}{2}$, we need no additional expansion for the $s_i$ since equation II(2.9) tells us that $s_i = -w_i$ for all $i$. But what happens in the case $\kappa \neq \frac{1}{2}$? We propose a modification, generalizing that used by Pierson & Fife (1961). We take

$$\kappa = \frac{1}{2} + \sum_{n=1}^{\infty} A_n \epsilon^n, \tag{2.8}$$

where the $A_n$ are all real. This has no effect on the governing equations. The expansion for the $s_i$ can then be computed from equations (2.5), (2.8) and II(2.9). We drop the hats from the $\hat{\alpha}_{ij}$, $\hat{\beta}_{ij}$, etc., for simplicity. No confusion with II will arise by so doing. Then we substitute equations (2.1)–(2.8) into equations II(2.9)–(2.11) and compare coefficients of $\epsilon$. This can be made easier by considering the cases $i$ (even) and $i$ (odd) separately. In addition, the following simplifications are useful (for $l$, $n$ integers):

$$\mathrm{int}(\tfrac{1}{2}(l+1)) = \tfrac{1}{2}l + \tfrac{1}{4}[1-(-1)^l], \tag{2.9}$$

$$\mathrm{int}(\tfrac{1}{2}(l+1)) + \mathrm{int}(\tfrac{1}{2}(l+n+1)) - 2 = \begin{cases} l + \frac{1}{2}(n-3), & n \text{ odd}, \\ 2\,\mathrm{int}(\frac{1}{2}(l+1)) + \frac{1}{2}(n-4), & n \text{ even}, \end{cases} \tag{2.10}$$

$$\mathrm{int}(\tfrac{1}{2}(l+1)) + \mathrm{int}(\tfrac{1}{2}(n-l+1)) - 2 = \begin{cases} \frac{1}{2}(n-3), & n \text{ odd}, \\ 2\,\mathrm{int}(\frac{1}{2}(l+1)) + \frac{1}{4}(n-4) - l, & n \text{ even}. \end{cases} \tag{2.11}$$

Eventually we arrive at the following sets of equations

$$\left( \text{N.B.} \sum_{n=1}^{N}{}^{*} a_n = a_1 + a_3 + a_5 + \ldots + \begin{cases} a_N, & N \text{ odd}, \\ a_{N-1}, & N \text{ even} \end{cases} \right):$$

$$\zeta_{0k} = -\gamma_{k-1} + \sum_{l=1}^{k} \delta_{l-1} \beta_{0,k-l+1} - 2 \sum_{l=1}^{k-1} A_l \zeta_{0,k-l} - 2 \sum_{n=1}^{k-2}{}^{*} \sum_{l=1}^{k-n-1} \left[ \frac{1}{n} \alpha_{nl} \beta_{n,k-n-l} + \frac{1}{(n+1)} \alpha_{n+1,l} \beta_{n+1,k-n-l} \right] \quad (k = 1, 2, \ldots), \tag{2.12}$$

$$\tfrac{1}{2}\zeta_{nk} = \sum_{l=1}^{k} \delta_{l-1}\beta_{n,k-l+1} - \sum_{l=1}^{n} \frac{1}{l} \sum_{j=1}^{k} \alpha_{lj}\beta_{n-l,k-j+1} - \sum_{l=1}^{k-1} A_l \zeta_{n,k-l}$$
$$- \sum_{m=1}^{k-1} \sum_{l=1}^{k-m} \left[\frac{1}{m}\alpha_{ml}\beta_{n+m,k-m-l+1} + \frac{1}{(m+n)}\alpha_{m+n,l}\beta_{m,k-m-l+1}\right]$$
$$(n = 1, 3, \ldots,\ k = 1, 2, \ldots), \quad (2.13)$$

$$\tfrac{1}{2}\zeta_{nk} = \sum_{l=1}^{k} \delta_{l-1}\beta_{n,k-l+1} - \sum_{l=2}^{n}{}^{*} \frac{1}{l} \sum_{m=1}^{k} \alpha_{lm}\beta_{n-l,k-m+1}$$
$$- \sum_{l=1}^{n-1}{}^{*} \frac{1}{l} \sum_{m=1}^{k-1} \alpha_{lm}\beta_{n-l,k-m} - \sum_{l=1}^{k-1} A_l \zeta_{n,k-l}$$
$$- \sum_{m=1}^{k-2}{}^{*} \sum_{l=1}^{k-m-1} \left\{\frac{1}{m}\alpha_{ml}\beta_{m+n,k-m-l} + \frac{1}{(m+1)}\alpha_{m+1,l}\beta_{m+n+1,k-m-l}\right.$$
$$\left. + \frac{1}{(m+n)}\alpha_{m+n,l}\beta_{m,k-m-l} + \frac{1}{(m+n+1)}\alpha_{m+n+1,l}\beta_{m+1,k-m-l}\right\}$$
$$(n = 2, 4, \ldots,\ k = 1, 2, \ldots), \quad (2.14)$$

$$\beta_{01} = 1,$$

$$\beta_{0j} = \sum_{n=1}^{j-2}{}^{*} \sum_{l=1}^{j-n-1} [\alpha_{nl}\alpha_{n,j-n-l} + \alpha_{n+1,l}\alpha_{n+1,j-n-l}] \quad (j = 2, 3, \ldots), \quad (2.15)$$

$$\beta_{nj} = \alpha_{nj} + \sum_{m=1}^{j-1} \sum_{l=1}^{j-m} \alpha_{ml}\alpha_{n+m,j-m-l+1} \quad (n = 1, 3, \ldots,\ j = 1, 2, \ldots), \quad (2.16)$$

$$\beta_{nj} = \alpha_{nj} + \sum_{m=1}^{j-2}{}^{*} \sum_{l=1}^{j-m-1} [\alpha_{ml}\alpha_{m+n,\,j-m-l} + \alpha_{m+1,l}\alpha_{m+n+1,j-m-l}]$$
$$(n = 2, 4, \ldots,\ j = 1, 2, \ldots), \quad (2.17)$$

$$\beta_{0j} = \sum_{m=1}^{j} \tau_{0m}\tau_{0,j-m+1} + \frac{1}{2} \sum_{n=1}^{j-2}{}^{*} \sum_{l=1}^{j-n-1} [\tau_{nl}\tau_{n,j-n-l} + \tau_{n+1,l}\tau_{n+1,j-n-l}] \ (j = 1, 2, \ldots), \quad (2.18)$$

$$\beta_{nl} = \sum_{m=1}^{l} \tau_{nm}\tau_{0,l-m+1} + \frac{1}{2} \sum_{m=1}^{l-1} \sum_{p=1}^{l-m} \tau_{mp}\tau_{n+m,l-m-p+1}$$
$$+ \frac{1}{4} \sum_{k=1}^{n-1} \sum_{j=1}^{l} \tau_{kj}\tau_{n-k,l-j+1} \quad (n = 1, 3, \ldots,\ l = 1, 2, \ldots), \quad (2.19)$$

$$\beta_{nl} = \sum_{m=1}^{l} \tau_{nm}\tau_{0,i-m+1} + \frac{1}{4} \sum_{k=2}^{n-2}{}^{*} \sum_{m=1}^{l} \tau_{km}\tau_{n-k,\,l-m+1} + \frac{1}{4} \sum_{k=1}^{n-1}{}^{*} \sum_{m=1}^{l-1} \tau_{km}\tau_{n-k,\,l-m}$$
$$+ \frac{1}{2} \sum_{m=1}^{l-2}{}^{*} \sum_{j=1}^{l-m-1} [\tau_{mj}\tau_{m+n,l-m-j} + \tau_{m+1,j}\tau_{m+n+1,l-m-j}]$$
$$(n = 2, 4, \ldots,\ l = 1, 2, \ldots); \quad (2.20)$$

$$\mu_{0j} = \sum_{n=1}^{j-2}{}^{*} \sum_{l=1}^{j-n-1} [n\alpha_{nl}\alpha_{n,j-n-l} + (n+1)\alpha_{n+1,l}\alpha_{n+1,j-n-l}] \quad (j = 1, 2, \ldots), \quad (2.21)$$

$$\mu_{nj} = n\alpha_{nj} + \sum_{m=1}^{j-1} (n+2m) \sum_{p=1}^{j-m} \alpha_{m+n,p}\alpha_{m,j-m-p+1} \quad (n = 1, 3, \ldots,\ j = 1, 2, \ldots), \quad (2.22)$$

$$\mu_{nj} = n\alpha_{nj} + \sum_{m=1}^{j-2}{}^{*} \sum_{l=1}^{j-m-1} [(n+2m)\alpha_{n+m,l}\alpha_{m,j-m-l}$$
$$+ (n+2m+2)\alpha_{n+m+1,l}\alpha_{m+1,j-m-l}] \quad (n = 2, 4, \ldots,\ j = 1, 2, \ldots), \quad (2.23)$$

$$\mu_{0j} = \sum_{m=1}^{j} \zeta_{0m}\tau_{0,j-m+1} + \frac{1}{2}\sum_{n=1}^{j-2}{}^{*} \sum_{l=1}^{j-n-1} [\zeta_{nl}\tau_{n,j-n-l} + \zeta_{n+1,l}\tau_{n+1,j-n-l}] \quad (j = 1, 2, \ldots), \tag{2.24}$$

$$\begin{aligned}\mu_{nl} = {} & \sum_{m=1}^{l} [\zeta_{nm}\tau_{0,l-m+1} + \zeta_{0m}\tau_{n,l-m+1}] \\ & + \frac{1}{2}\sum_{m=1}^{l-1} \sum_{p=1}^{l-m} [\zeta_{mp}\tau_{n+m,l-m-p+1} + \zeta_{m+n,p}\tau_{m,l-m-p+1}] \\ & + \frac{1}{2}\sum_{k=1}^{n-1} \sum_{j=1}^{l} \zeta_{kj}\tau_{n-k,l-j+1} \quad (n = 1, 3, \ldots,\ l = 1, 2, \ldots),\end{aligned} \tag{2.25}$$

$$\begin{aligned}\mu_{nl} = {} & \sum_{m=1}^{l} [\zeta_{nm}\tau_{0,l-m+1} + \zeta_{0m}\tau_{n,l-m+1}] \\ & + \frac{1}{2}\sum_{m=1}^{l-2}{}^{*} \sum_{j=1}^{l-m-1} \{\zeta_{mj}\tau_{m+n,l-m-j} + \zeta_{m+1,j}\tau_{m+n+1,l-m-j} + \zeta_{m+n,j}\tau_{m,l-m-j} \\ & + \zeta_{m+n+1,j}\tau_{m+1,l-m-j}\} + \frac{1}{2}\sum_{k=2}^{n-2}{}^{*} \sum_{m=1}^{l} \zeta_{km}\tau_{n-k,l-m+1} \\ & + \frac{1}{2}\sum_{k=1}^{n-1}{}^{*} \sum_{m=1}^{l-1} \zeta_{km}\tau_{n-k,l-m} \quad (n = 2, 4, \ldots,\ l = 1, 2, \ldots).\end{aligned} \tag{2.26}$$

Here the summation is taken to be identically zero, if the lower limit exceeds the upper. Equation (2.12) is equivalent to II(3.2$a$), (2.13) and (2.14) to II(3.2$b$), (2.15) to II(3.2$c$), (2.16) and (2.17) to II(3.2$d$), (2.18) to II(3.2$e$), (2.19) and (2.20) to II(3.2$f$), (2.21) to II(3.2$g$), (2.22) and (2.23) to II(3.2$h$), (2.24) to II(3.2$j$), (2.25) and (2.26) to II(3.2$k$). Again, as in II, §3, this set of equations is closed only when we define the parameter $\epsilon$.

### (*b*) *Correction and extension of Wilton's work*

By letting $\epsilon = a_1$ and $A_n = 0$ for all $n$ in equation (2.8), we can check Wilton's expansions for $\kappa = \frac{1}{2}$. From (2.1) this means we must take

$$\alpha_{11} = 1, \quad \alpha_{1n} = 0 \quad (n = 2, 3, \ldots) \tag{2.27}$$

and we find that, correct to the given order,

$$a_2 = \pm a_1 - \tfrac{1}{4}a_1^2 + O(a_1^3), \tag{2.28}$$

$$a_3 = \mp \tfrac{9}{4}a_1^2 - \tfrac{45}{8}a_1^3 + O(a_1^4), \tag{2.29}$$

$$a_4 = 0 + O(a_1^4), \tag{2.30}$$

$$a_5 = -\tfrac{25}{16}a_1^3 + O(a_1^4), \tag{2.31}$$

$$a_6 = \mp \tfrac{9}{40}a_1^3 + O(a_1^4), \tag{2.32}$$

$$c^2 = \tfrac{3}{2} \pm \tfrac{3}{4}a_1 - \tfrac{33}{16}a_1^2 + O(a_1^3), \tag{2.33}$$

$$K = \tfrac{3}{2} \pm \tfrac{3}{4}a_1 - \tfrac{9}{16}a_1^2 + O(a_1^3). \tag{2.34}$$

Equations (2.28)–(2.34) do not all agree with Wilton's, even when due account is taken of notational changes. Equations (2.30), (2.31) (and consequently (2.33),

(2.34)) disagree. However, the fault lies in Wilton's work, as can easily be seen by substituting his expressions (near the bottom of page 698) into his equation (9). The left-hand side is non-zero. With the equations (2.28)–(2.34) above, Wilton's equation (9) *is* satisfied. In addition, Wilton's expressions for $K$ and $c^2$ can be shown to lead to negative values for the kinetic energy (use equation II (3.10)). The top (bottom) sign corresponds to the gravity- (capillary-) side solution obtained by Chen & Saffman. At this point we change slightly the terminology of Chen & Saffman. The terms 'gravity-side' and 'capillary-side' tend to imply one sort of behaviour on one side of $\kappa = 1/n$ and another sort on the other side. This is not the case, as they have shown. We prefer the terms 'gravity-like' and 'capillary-like', as used by Rottman & Olfe. We shall see that these waves possess properties normally associated with pure gravity ($\kappa = 0$) or pure capillary ($\kappa$ infinite) waves.

But the choice of $\epsilon = a_1$ is not usually, as explained in II, §3, the best possible. So to consider combination (2, 1) gravity- and capillary-like waves we choose $\epsilon = h$, where $h$ is the wave amplitude. From (2.1), this requires us to take the following

$$\alpha_{11} = 1, \quad \alpha_{1n} = -\sum_{j=2}^{n} \frac{\alpha_{2j-1,\,n-j+1}}{(2j-1)} \tag{2.35}$$

(compare with II (3.6)).

This choice of $\epsilon$ leads to the following expressions for $a_n$, correct to the given order, for $\kappa = \frac{1}{2}$:

$$a_1 = h \pm \tfrac{3}{4}h^2 + \tfrac{53}{16}h^3 \pm \tfrac{977009}{96000}h^4 + O(h^5), \tag{2.36}$$

$$a_2 = \pm h + \tfrac{1}{2}h^2 \pm \tfrac{5}{3}h^3 + \tfrac{295499}{96000}h^4 + O(h^5), \tag{2.37}$$

$$a_3 = \mp \tfrac{9}{4}h^2 - 9h^3 \mp \tfrac{927}{32}h^4 + O(h^5), \tag{2.38}$$

$$a_4 = \tfrac{22767}{6000}h^4 + O(h^5), \tag{2.39}$$

$$a_5 = -\tfrac{25}{16}h^3 \mp \tfrac{4312}{128}h^4 + O(h^5), \tag{2.40}$$

$$a_6 = \mp \tfrac{9}{40}h^3 + \tfrac{70833}{16000}h^4 + O(h^5), \tag{2.41}$$

$$c^2 = \tfrac{3}{2} \pm \tfrac{3}{4}h - \tfrac{3}{2}h^2 \mp \tfrac{219}{64}h^3 - \tfrac{5704553}{384000}h^4 + O(h^5), \tag{2.42}$$

$$K = \tfrac{3}{2} \pm \tfrac{3}{4}h \mp \tfrac{91}{64}h^3 - \tfrac{1608553}{384000}h^4 + O(h^5). \tag{2.43}$$

We note the continued absence of terms in $h^2$, $h^3$ in the expansion of $a_4$, and attribute this to the higher ordering of $a_2$. The missing term in $h^2$ in $K$ is due to the particular choice of $\epsilon$. Again, the top (bottom) sign refers to a gravity (capillary) type of solution. In addition, for $\kappa \doteqdot \frac{1}{2}$ if we set $A_n = 0$ for $n \geqslant 2$, to simplify ideas, we find:

$$a_1 = h + (\tfrac{1}{2}A_1 \pm (\tfrac{9}{16} + \tfrac{1}{4}A_1^2)^{\frac{1}{2}})\,h^2 + O(h^3), \tag{2.44}$$

$$a_2 = (\tfrac{2}{3}A_1 \pm (1 + \tfrac{4}{9}A_1^2)^{\frac{1}{2}})\,h + O(h^2), \tag{2.45}$$

$$a_3 = (-\tfrac{3}{2}A_1 \mp (\tfrac{81}{16} + \tfrac{9}{4}A_1^2)^{\frac{1}{2}})\,h^2 + O(h^3), \tag{2.46}$$

$$c^2 = \tfrac{3}{2} + (\tfrac{3}{2}A_1 \pm (\tfrac{9}{16} + \tfrac{1}{4}A_1^2)^{\frac{1}{2}})\,h + O(h^2), \tag{2.47}$$

$$K = \tfrac{3}{2} + (\tfrac{3}{2}A_1 \pm (\tfrac{9}{16} + \tfrac{1}{4}A_1^2)^{\frac{1}{2}})\,h + O(h^2). \tag{2.48}$$

It was not considered worth while to carry this hand calculation further, since it is a *special* case of equation (2.8). In addition, we state without proof that if a term of

$O(1)$, say $A_0$, is added to the right-hand side of equation (2.8), it can be shown that $A_0 \equiv 0$, as we might expect since the perturbation is about $\kappa = \frac{1}{2}$. To order $h$, it is not possible to have $a_N = 0$ $(N = 1, \ldots, M-1)$, $a_M \neq 0$ $(M > 1)$ in equations (2.44) and (2.45). Thus we have temporarily excluded waves of degree $M$, in the region of $\kappa = \frac{1}{2}$, from our formulation.

Equations (2.12)–(2.26) and (2.35) are then programmed onto a computer as indicated in II, §3, the algorithm being given in Hogan (1979*b*). A quadruple precision solution up to $O(h^{42})$ takes approximately fourteen minutes to execute (as opposed to ten minutes in II, §3). The lower order in this section is actually fictitious. In II, the expansion was in $h^2$; here it is in $h$.

Runs are made with both choices of sign, with no difference in execution time. It could be argued that it would be simpler to change the sign of each alternate term in one run in order to get the results for the next one (a simple matter in modern computer filing systems). It is, however, an additional test of the computer program that *two* runs should be made with the comparison done afterwards. The results agree exactly with those given in equations (2.36)–(2.48).

### (c) *Integral property expansions*

Now that we have the $\alpha_{ij}$, etc., we can calculate the $a_i$, etc., using equations (2.1)–(2.7). We have the same general expressions for $\bar{\eta}$, $T$, $I$, $V$, $S_{xx}$, $S_{zz}$ and $F$ as in II, but the actual form of their expansions is different. In particular we now have

$$\bar{\eta} = \frac{1}{2}\sum_{j=2}^{\infty}(\delta_j - \gamma_j)h^j, \tag{2.49}$$

$$T = \frac{1}{4}\sum_{j=2}^{\infty}\sum_{k=0}^{j}\gamma_{j-k}(\delta_k - \gamma_k)h^j, \tag{2.50}$$

$$V_\tau = \kappa\sum_{j=2}^{\infty}\tau_{0,j+1}h^j, \tag{2.51}$$

$$\begin{aligned}
V_g = {} & \frac{1}{4}\sum_{m=2}^{\infty}\sum_{n=1}^{m-1}{}^{*}\sum_{l=1}^{m-n}\left[\frac{1}{n^2}\alpha_{nl}\alpha_{n,m-n-l+1} + \frac{1}{(n+1)^2}\alpha_{n+1,l}\alpha_{n+1,m-n-l+1}\right]h^m \\
& + \frac{1}{8}\sum_{i=2}^{\infty}\sum_{s=1}^{i}{}^{*}\sum_{r=1}^{\frac{1}{2}(s+1)}\sum_{k=1}^{i-s}\sum_{j=1}^{i-s-k}\left[\frac{1}{(s-2r+2)} + \frac{2}{(s+1)}\right] \\
& \times \frac{\alpha_{s+1,k}\alpha_{2r-1,j}\alpha_{s-2r+2,i-s-k-j+1}}{(2r-1)}h^i \\
& + \frac{1}{2}\sum_{i=2}^{\infty}\sum_{s=2}^{i}{}^{*}\sum_{r=1}^{\frac{1}{2}s}\sum_{k=1}^{i-s}\sum_{j=1}^{i-s-k}\left\{\left[\frac{1}{(s-2r+2)} + \frac{2}{(s+1)}\right]\right. \\
& \times \frac{\alpha_{s+1,k}\alpha_{2r-1,j}\alpha_{s-2r+2,i-s-k-j+1}}{(2r-1)} \\
& + \left[\frac{1}{(s-2r+1)} + \frac{2}{(s+1)}\right]\frac{\alpha_{s+1,k}\alpha_{2r,j}\alpha_{s-2r+1,i-s-k-j+1}}{2r} \\
& \left. + \left[\frac{1}{(s-2r+2)} + \frac{2}{(s+2)}\right]\frac{\alpha_{s+2,k}\alpha_{2r,j}\alpha_{s-2r+2,i-s-k-j+1}}{2r}\right\}h^i
\end{aligned}$$

$$-\frac{1}{8}\sum_{k=2}^{\infty}\sum_{l=1}^{k-1}\left[\sum_{n=1}^{l-1\,*}\sum_{m=1}^{l-n}\left[\frac{1}{n}\alpha_{nm}\alpha_{n,\,l-n-m+1}+\frac{1}{(n+1)}\alpha_{n+1,\,m}\alpha_{n+1,\,l-n-m+1}\right]\right]$$

$$\times\left[\sum_{n=1}^{k-l-1\,*}\sum_{m=1}^{k-l-n}\left[\frac{1}{n}\alpha_{nm}\alpha_{n,\,k-l-n-m+1}+\frac{1}{(n+1)}\alpha_{n+1,\,m}\alpha_{n+1,\,k-l-n-m+1}\right]\right]h^k. \quad (2.52)$$

Equations (2.50)–(2.52) are to be compared with equations II(3.13)–(3.15). The general forms of the radiation stresses $S_{xx}$, $S_{zz}$ and the energy flux $F$ are not given (see equations II (3.16)–(3.18)).

The following expressions are then obtained, for $\kappa = \frac{1}{2}$;

$$T = \tfrac{9}{16}h^2 \pm \tfrac{33}{32}h^3 + \tfrac{61}{16}h^4 + O(h^5), \quad (2.53)$$

$$V = \tfrac{9}{16}h^2 \pm \tfrac{15}{16}h^3 + 4h^4 + O(h^5), \quad (2.54)$$

$$S_{xx} = \tfrac{17}{16}h^2 \pm \tfrac{29}{16}h^3 + \tfrac{731}{96}h^4 + O(h^5), \quad (2.55)$$

$$S_{zz} = \pm\tfrac{3}{32}h^3 - \tfrac{3}{16}h^4 + O(h^5), \quad (2.56)$$

$$\frac{F}{c} = \tfrac{17}{16}h^2 \pm \tfrac{55}{32}h^3 + \tfrac{749}{96}h^4 + O(h^5). \quad (2.57)$$

From equations II(3.19)–(3.23), we would expect that

$$T = V = \tfrac{3}{8}h^2 \quad \text{and} \quad S_{xx} = F/c = \tfrac{5}{6}h^2,$$

when $\kappa = \frac{1}{2}$. However, that is for a linear wave with profile $y = h\cos x$. Here we have $y = h\cos x \pm \frac{1}{2}h\cos 2x$, and so different first-order values for the integral properties must be expected. In addition, we note that $S_{zz}$ (and hence the average Lagrangian $\mathscr{L} \equiv T - V$) is now $O(h^3)$, whereas beforehand it was $O(h^4)$. $S_{zz}$ is also positive (negative) for the gravity- (capillary-) like solution. This is to be compared with the properties of $S_{zz}$ in II, §3. There $S_{zz} \gtrless 0$ for $\kappa \lesseqgtr \frac{1}{2}$.

Of course it is possible to obtain expansions of the integral properties for $\kappa \doteqdot \frac{1}{2}$ similar to equations (2.53)–(2.57) by using equations (2.49)–(2.52), etc. But for these near-resonance waves we shall show that the phase speed $c$ and the wave profiles prove to be quite sufficient to gauge the behaviour of other quantities.

We use equation (2.8) as follows: for a given value of $\kappa$ we choose the same number of non-zero $A_n$ as the number of heights in which we are interested. So for example with $N$ heights and $\kappa = \kappa_1$ we set $A_n = 0$ for $n \geqslant N+1$, and equation (2.8) is evaluated $N$ times to give $N$ linear simultaneous equations in $N$ unknowns $(A_1 - A_N)$. Then, using results analogous to equations (2.44)–(2.48), we calculate the required properties, at each of the prescribed heights. Evaluation at other values of $h$ would mean that $\kappa \neq \kappa_1$, although the results would be just as valid. For example, take $\kappa = 0{\cdot}4$ and $h = 0{\cdot}01, 0{\cdot}05, 0{\cdot}1$. Then $A_1 = -1{\cdot}3 \times 10^1$, $A_2 = 3{\cdot}2 \times 10^2$, $A_3 = -2{\cdot}0 \times 10^3$, and $A_n = 0$ $(n \geqslant 4)$ solves equation (2.8) for the given values of $\kappa$ and $h$. However, if $h = 0{\cdot}001$, then $\kappa = 0{\cdot}487318$. This can place restrictions on the procedure. Nevertheless, valuable results can still be obtained, as we shall see in §3.

With $A_n = 0$ for $n \geqslant 2$, $A_1 > 0\,(< 0)$ corresponds to the graphs $\kappa > \frac{1}{2}\,(< \frac{1}{2})$ in figure 4 of Chen & Saffman (1979). Only the curved sections of these graphs can be reached when using equations (2.44) and (2.45). The region $OB$ is inaccessible, with

$$OB \doteqdot \tfrac{4}{3}A_1 h. \quad (2.58)$$

### (*d*) *Waves of degree 2 or more*

The perturbation expansion, advocated in equations (2.1)–(2.7), can deal with waves of a given degree at $\kappa = \frac{1}{2}$. We must consider a degree of 2 or more, because waves of degree 1 have singularities at $\kappa = \frac{1}{2}$; see II, equation (3.7). Let us take the degree to be 2 and then $\epsilon = \pm a_2$ and $a_1 = 0$. So, from equation (2.1), we must set

$$\alpha_{21} = \pm 1, \quad \alpha_{2m} = \alpha_{1n} = 0 \quad (m = 2, 3, \ldots, \quad n = 1, 2, \ldots). \tag{2.59}$$

Equations (2.12)–(2.26), together with equation (2.59), then give us:

$$a_1 = 0, \quad a_2 = a_2, \tag{2.60}$$

$$a_3 = 0 + O(a_2^4), \tag{2.61}$$

$$a_4 = 0 + O(a_2^4), \tag{2.62}$$

$$a_5 = 0 + O(a_2^4), \tag{2.63}$$

$$a_6 = \mp \tfrac{9}{40} a_2^3 + O(a_2^4), \tag{2.64}$$

$$c^2 = \tfrac{3}{2} - \tfrac{3}{8} a_2^2 + O(a_2^3), \tag{2.65}$$

$$K = \tfrac{3}{2} + \tfrac{1}{8} a_2^2 + O(a_2^3). \tag{2.66}$$

We expect the remaining coefficients of $a_3$ and $a_5$ to vanish. This is not the case for $a_4$, where $\alpha_{41} = \alpha_{42} = 0$ independent of the value of $\alpha_{11}$ and $\alpha_{21}$. Equations (2.60)–(2.66) represent waves of degree 2 at $\kappa = \frac{1}{2}$. The solution algorithm has to be slightly modified to deal with this case. See Hogan (1979*b*) for full details. Hence, our perturbation expansionis capable of dealing with waves of a given degree at $\kappa = \frac{1}{2}$.

## 3. Results for exact resonance ($\kappa = \frac{1}{2}$) and near-resonance ($\kappa \doteqdot \frac{1}{2}$) waves

We are now able to discuss the properties of (2, 1) combination waves which occur at and near $\kappa = \frac{1}{2}$. One type comes from taking the upper sign in equations (2.44)–(2.48), the other one from the lower. Also we shall show that describing the former as gravity-like and the latter as capillary-like turns out to be completely vindicated, at least for small steepnesses.

Generally it was found that the series (2.1)–(2.7) were very slowly convergent. Even Padé approximants proved unhelpful as $\epsilon$ increased. The ratio of successive terms in each series behaved in an oscillatory manner which appeared to tend to a limit beyond $h^{130}$. It proved impossible to obtain this number of terms owing to the size of the computational facilities available. In fact, the author could not obtain all coefficients of $h^{43}$. The size of these coefficients was not a limiting factor with those multiplying $h^{130}$ expected to be $O(10^{67})$.

This situation is quite unlike that discussed in II where the ratio of successive coefficients monotonically approached a limit, which was the same for each series summed for a given value of $\kappa$.

The results in this section, therefore, should be interpreted with care near $\epsilon = h = h_{\max}$, with accuracy of only one decimal place assumed at $h = h_{\max}$. The profiles and properties of the waves are not affected qualitatively.

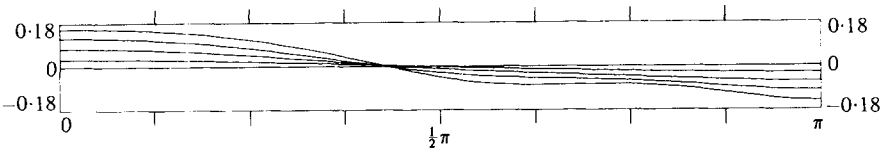


FIGURE 1. Wave profiles, in the case $\kappa = 0{\cdot}3$, for $h = 0{\cdot}03, 0{\cdot}07, 0{\cdot}11, 0{\cdot}15$. The still water line is included for reference.

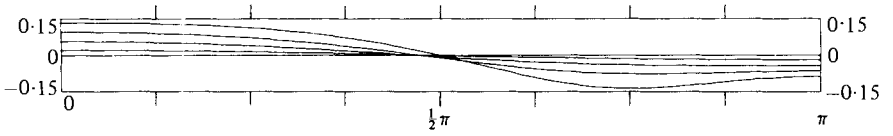


FIGURE 2. Wave profiles, in the case $\kappa = 0{\cdot}4$, for $h = 0{\cdot}02, 0{\cdot}05, 0{\cdot}08, 0{\cdot}11$. The still water line is included for reference.

### (*a*) *Wave profiles*

With the $\alpha_{ij}$ already found in §2, we can construct a set of $a_i$ for the required values of $h$, using equation (2.1) and $\epsilon = h$. Other coefficients we will use are $\delta_i$, $\gamma_i$ and $\tau_{0i}$ – similar to those used in II. We can draw wave profiles and calculate integral properties with these coefficients. In the case of capillary-like combination (2, 1) waves at $\kappa = \frac{1}{2}$, we will compare results with the values $\kappa = 0{\cdot}6, 0{\cdot}8$ as described in II. For the gravity-like waves, comparison is made with $\kappa = 0{\cdot}3, 0{\cdot}4$, again computed as in II. A wave with $\kappa = 0{\cdot}8$ looks very similar to one with $\kappa = 1{\cdot}0$, as shown in II, figure 13, and its properties have been fully detailed in II, table 5. The same is not true for $\kappa = 0{\cdot}6$. As we have already remarked in §1, convergence could not be obtained for $h \geqslant 0{\cdot}3$, owing to the proximity of $\kappa$ to $\frac{1}{2}$. The profiles which could be drawn were very similar to $\kappa = 1{\cdot}0$, except that a dip developed in the crest for $h > 0{\cdot}2$, approximately. The wave properties are presented in this section. For $\kappa = 0{\cdot}3, 0{\cdot}4$ the half-wavelength profiles obtained by this method are shown in figures 1 and 2 respectively. When $\kappa = 0{\cdot}3$, we note the appearance of two extra troughs (over one wavelength) as $h$ increases (for $h \geqslant 0{\cdot}13$). But, when $\kappa = 0{\cdot}4$, one extra crest appears in the trough (for $h \geqslant 0{\cdot}05$). Nothing exceptional happens at the crests of either set of waves. In each case it is tempting to believe that eventually the highest wave may be trough limited (i.e. a bubble may form). From the work of other authors this seems to be the case. In fact, each wave is both capillary- and gravity-like (see later). We shall retain the term gravity-like for simplicity. It should be noted that $\kappa = 0{\cdot}4$ is almost midway between $\kappa = \frac{1}{2}$ and $\kappa = \frac{1}{3}$ singularities and $\kappa = 0{\cdot}3$ is similarly situated between $\kappa = \frac{1}{3}$ and $\kappa = \frac{1}{4}$ singularities. Chen & Saffman (1980) give profiles of (2, 1) combination waves for $\kappa = 0{\cdot}3$, in their figure 3. The wave is very much like Crapper's pure capillary wave, with the highest enclosing a bubble of air and $h_{\max} = 0{\cdot}4305$. The waves in figures 1 and 2 are pure waves of degree 1, for small amplitudes.

For the near-resonance waves we consider five cases in detail, using equation (2.8). They are $A_1 = \pm\frac{1}{100}$, $A_1 = \pm 1$ and $A_1 = \frac{1}{2}$ with $A_n = 0$ $(n \geqslant 2)$ in each case. The first two values of $A_1$ are used to determine the behaviour of the wave near $\kappa = \frac{1}{2}$ and the last three values are used as a check on the accuracy of the method.

Let us consider the lower sign results of equations (2.44)–(2.48) together with $A_1 = +\frac{1}{100}$, exact resonance ($A_1 = 0$) and $A_1 = -\frac{1}{100}$. The wave profile results are

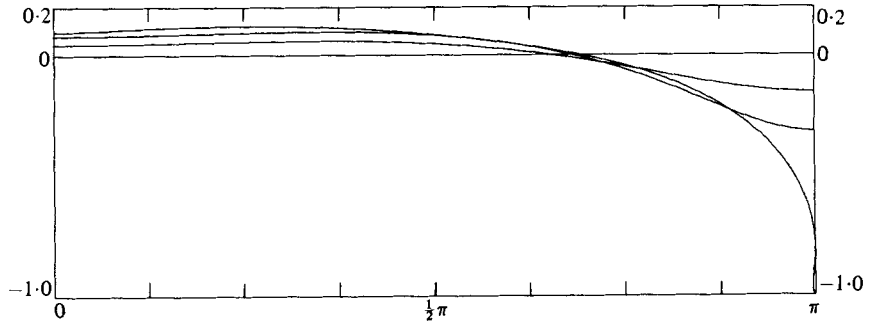


FIGURE 3. Capillary-like wave profiles, in the case $A_1 = \frac{1}{100}$, for $h = 0{\cdot}1, 0{\cdot}2, 0{\cdot}5484$.

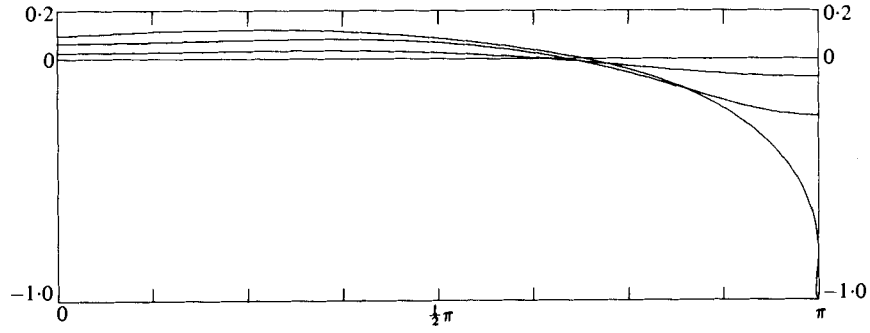


FIGURE 4. Capillary-like wave profiles, in the case $\kappa = 0{\cdot}5$, for $h = 0{\cdot}05, 0{\cdot}15, 0{\cdot}5450$.

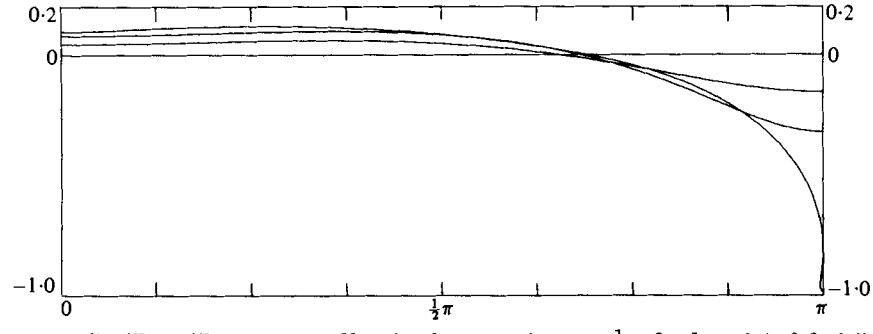


FIGURE 5. Capillary-like wave profiles, in the case $A_1 = -\frac{1}{100}$, for $h = 0{\cdot}1, 0{\cdot}2, 0{\cdot}5413$.

given in figures 3–5. Each highest wave is capillary-like, with a bubble enclosed in the trough. Note the dip in the crest, as in the case $\kappa = 0{\cdot}6$. For clarity of presentation, other wave heights have been omitted. Nevertheless, the crest height of the wave above the mean level is still a non-monotonic function of the wave height as we found in I, figure 4, for $\kappa$ infinite and II for $\kappa \geqslant 0{\cdot}8$. The values of $h_{\max}$ in each case are given in table 1, together with other values of $A_1$. It can be seen that these values fit in well with the known values for $\kappa = 0{\cdot}8$, $1{\cdot}0$ (II, table 1). However, as $|A_1|$ increases, the accuracy is expected to become impaired. $A_2$, $A_3$, etc., should be used to get a better 'fit' further away from $\kappa = \frac{1}{2}$. The value of $h_{\max}$ at $\kappa = \frac{1}{2}$ is slightly lower than Schwartz & Vanden-Broeck (1979) obtained in their study of the problem, because

| $\kappa$ | $h_{\max}$ | $A_1$ |
|---|---|---|
| 0·35 | 0·45 | −0·3333 |
| 0·38 | 0·47 | −0·2500 |
| 0·40 | 0·48 | −0·2000 |
| 0·42 | 0·49 | −0·1666 |
| 0·45 | 0·51 | −0·1000 |
| 0·47 | 0·52 | −0·0633 |
| 0·49 | 0·54 | −0·0200 |
| 0·50 | 0·55 | 0 |
| 0·51 | 0·55 | 0·0200 |
| 0·54 | 0·57 | 0·0633 |
| 0·56 | 0·58 | 0·1000 |
| 0·60 | 0·60 | 0·1666 |
| 0·62 | 0·62 | 0·2000 |
| 0·66 | 0·64 | 0·2500 |
| 0·72 | 0·67 | 0·3333 |

TABLE 1. Highest capillary-like waves for $\kappa \doteqdot \frac{1}{2}$, for various values of $A_1$; $A_n = 0\ (n \geqslant 2)$.

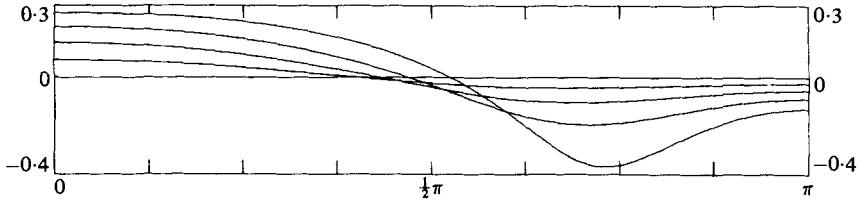


FIGURE 6. Gravity-like wave profiles, in the case $\kappa = 0{\cdot}5$, for $h = 0{\cdot}05, 0{\cdot}10, 0{\cdot}15, 0{\cdot}20$.

of the small number of terms used here. Rottman & Olfe (1979) did not obtain a highest capillary-like wave at $\kappa = \frac{1}{2}$, because their method is unable to describe waves with vertical tangents. Schwartz & Vanden-Broeck obtain $h_{\max} = 0{\cdot}622$ for $\kappa = 0{\cdot}6$. Our estimate is nearer 0·6, although it may change as other coefficients $A_n$ are included. It should be noted that figures 3 and 5 actually depict *three* values of $\kappa$ each, whereas figure 4 is only for $\kappa = \frac{1}{2}$. So for example in figure 3, when $h = 0{\cdot}1$, $\kappa = 0{\cdot}501$ and not $\kappa = 0{\cdot}502$ or 0·505484. However, this merely reinforces the continuity of the solution at $\kappa = \frac{1}{2}$.

The upper sign results of equations (2.44)–(2.48) are now considered, taking the cases $A_1 = +\frac{1}{100}$, exact resonance and $A_1 = -\frac{1}{100}$. Only the result for $A_1 = 0$ is given, in figure 6. The other profiles are almost exactly the same. Here, as in figure 2, convergence could not be obtained above a certain height (0·2 in the present case). Hence the highest wave in the gravity-like cases is still unknown. Schwartz & Vanden-Broeck produce wave profiles at $\kappa = \frac{1}{2}$, which are very similar to our figures 4 and 6 (their figures 4 and 5). Their 'wave of type 1 (2)' corresponds to our capillary- (gravity-) like solutions. Their gravity-like profile is higher than ours, although it is still not limited by a bubble in the trough. The same is true of the gravity-like wave at $\kappa = \frac{1}{2}$ drawn by Rottman & Olfe. Thus, even now, the exact shape of this highest wave is unknown. Chen & Saffman do not give profiles for waves with $\kappa = \frac{1}{2}$.

With these results (figures 3–6) we see the possibility of two waves existing at wavelengths other than $\kappa = \frac{1}{2}$. Some authors have neglected the gravity-like solution

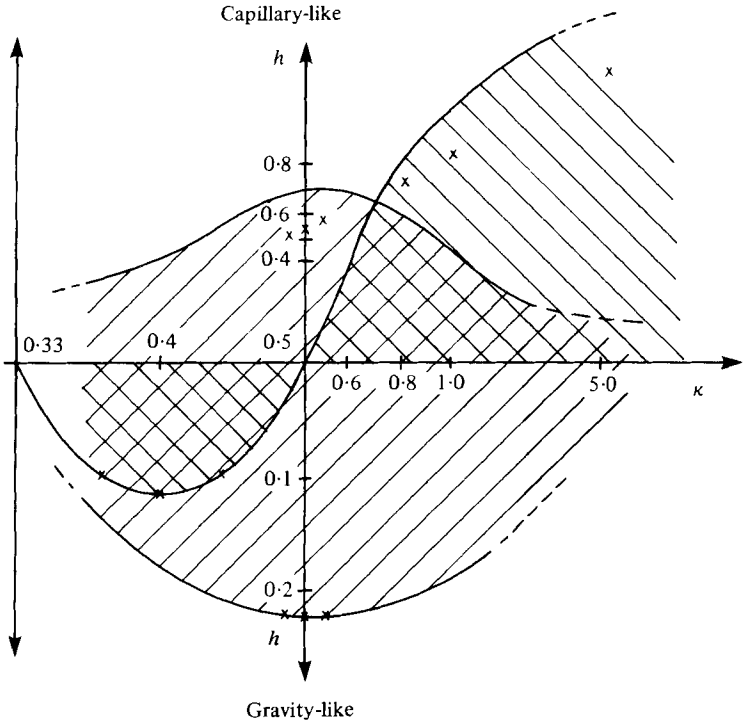


FIGURE 7. Validity regions for both capillary- and gravity-like solutions for both methods of computation. ×, highest wave calculated; ⧵⧵, region of solutions with $a_n$ expansion as used in II; ⫽, region of solutions with $\kappa - \frac{1}{2} = hA$, and present $a_n$ expansion; ▩, overlap region.

with $\kappa > \frac{1}{2}$, together with the capillary-like solution with $\kappa < \frac{1}{2}$, for reasons which do not seem obvious. But we can now see that both sorts of waves are sensible on both sides of $\kappa = \frac{1}{2}$, and no sound argument (based on stability or whatever) exists, at the moment, for rejecting any solution.

Wilton (1915) drew only two profiles for $\kappa = \frac{1}{2}$, corresponding to our figures 4 and 6 (his figures 4*b* and 4*a* respectively). Despite his algebraic errors and some convergence difficulties (partly overcome here by use of Padé approximants), he still found the crest in the trough of the gravity-like solution (at $h = 0{\cdot}06$) and the dip in the crest of the capillary-like solution (at $h = 0{\cdot}083$). However, he was not certain of the latter phenomenon and found no hint of a bubble in the capillary-like solution. Pierson & Fife (1961) have given profiles of waves at $\kappa = \frac{1}{2}$, in their figure 5. The profiles are similar to ours, except their gravity-like profile has a dip in its crest and their capillary-like profile has a dip just *before* the crest. In addition, they do not find a highest wave profile for the capillary-like solution. Pierson (1977, private communication), amongst others, has indicated that some of the expressions, used to draw the profiles, contain algebraic errors. Consequently, no significance can be attached to the difference we have found. Nayfeh (1970) is the only other author with whom comparison is possible. The top and middle curves of his figure 3 are very similar to those of Pierson & Fife, and different from our figures 4 and 6. Also, Nayfeh's expressions for the wave profile differ only slightly from those of Pierson & Fife.

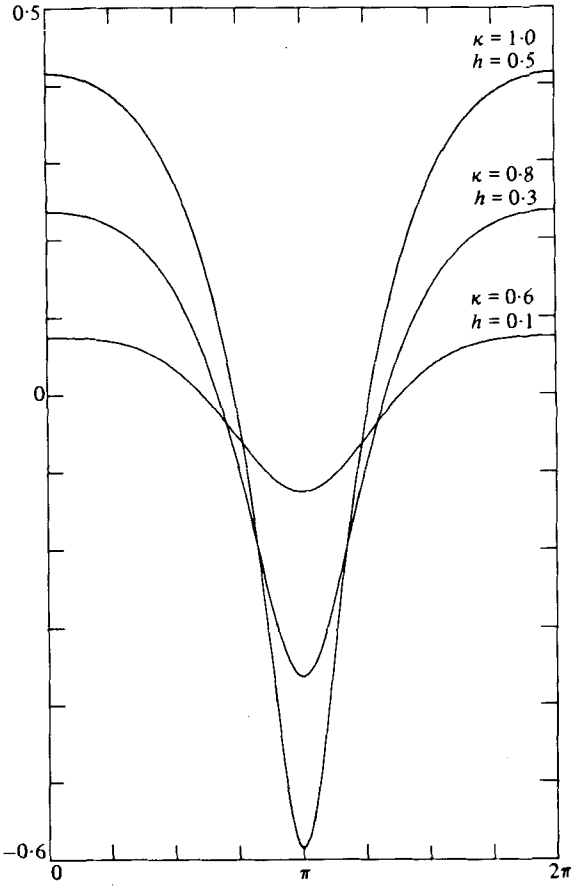


FIGURE 8. Three capillary-like waves, drawn by both methods, taken in the first quadrant of figure 7 with $A_1 = 1$. Vertical scaling exaggerated.

Consequently, they are suspect also. Wilton, Pierson & Fife and Nayfeh do not give near-resonant profiles.

### (*b*) *Validity regions and comparison of expansions*

As we have already mentioned, solutions exist on both sides of $\kappa = \frac{1}{2}$ for both types of wave. In addition, we have solutions from II which are valid away from $\kappa = \frac{1}{2}$. In the latter case, the radius of convergence is sometimes less than and sometimes greater than the highest wave for capillary-like solutions. We have taken the radius of convergence to represent the highest wave for gravity-like solutions. The regions of validity are summarized in figure 7, in schematic form.

By simply taking more terms in equation (2.8) we are able to extend the validity region of the 'new' $a_n$ expansion. Also we note that there are two overlap regions in which both methods produce solutions, and which should agree, since they represent the same wave. We now compare six waves, using three values of $A_1$ (with $A_n = 0$, $n \geqslant 2$).

In figure 8, with $A_1 = 1$, we have superimposed three waves $[(\kappa, h) = (1{\cdot}0, 0{\cdot}5), (0{\cdot}8, 0{\cdot}3), (0{\cdot}6, 0{\cdot}1)]$ obtained by one method, on top of the same three waves drawn

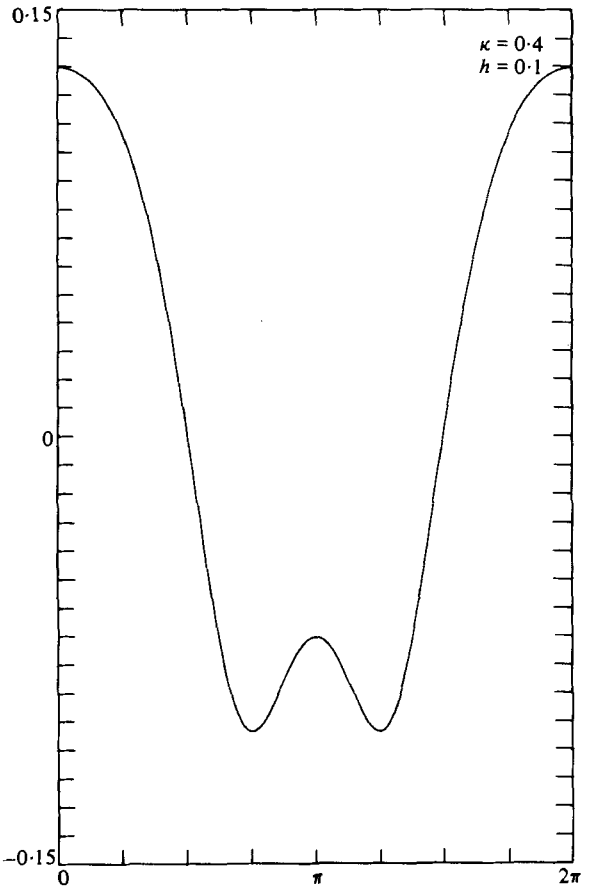


FIGURE 9. One gravity-like wave, drawn by both methods, taken in the third quadrant of figure 7 with $A_1 = -1$. Vertical scaling exaggerated.

by the other. Even with the vertical scale enlarged to emphasize differences, only three profiles can be seen. In figure 9, $A_1 = -1$, and one wave $[(\kappa, h) = (0{\cdot}4, 0{\cdot}1)]$ is drawn by the two methods. Again, there is no noticeable difference. Those values of $A_1$ ($\pm 1$) give profiles from both the overlap regions ($A_1 = 1$ in the first quadrant, $A_1 = -1$ in the third). The agreement is striking and represents a powerful endorsement of both methods of calculation. The higher waves, for a given $\kappa$, are not so well represented, as we see in figure 10. Here $A_1 = \frac{1}{2}$ and we are in the first quadrant. Four profiles are drawn; two each by the different methods for $(\kappa, h) = (0{\cdot}6, 0{\cdot}2)$ and $(0{\cdot}8, 0{\cdot}6)$. The agreement is worst at the crest and trough for both sets of $(\kappa, h)$. However, since $h_{\max} = 0{\cdot}7243$ for $\kappa = 0{\cdot}8$(II, table 1), it is better than could be expected from a one-term approximation so near to the highest wave. The dip in the crest at $(\kappa, h) = (0{\cdot}6, 0{\cdot}2)$ is just discernible. It is clear that taking more terms in equation (2.8) is likely to reproduce the highest wave for both values of $\kappa$. The crest and trough $y$ co-ordinates of the twelve profiles of the six waves given in figures 8–10 are presented in table 2.

Also, we can compare the phase speeds, using equations (2.47) and II(3.7$g$). We will give a fuller description of this property soon, but the comparison seems fitting

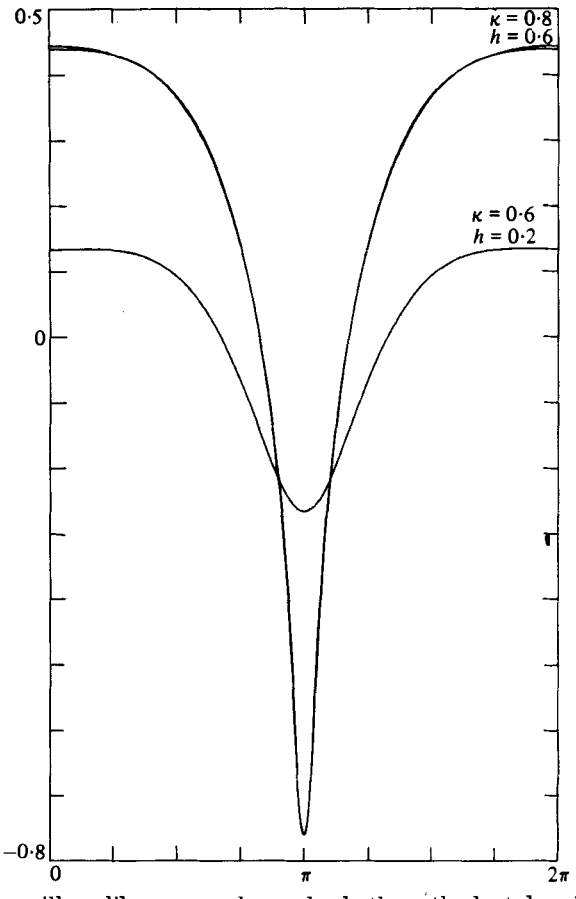


FIGURE 10. Two capillary-like waves, drawn by both methods, taken in the first quadrant of figure 7 with $A_1 = \frac{1}{2}$. Vertical scaling exaggerated.

| $\kappa$ | $h$ | Crest $y$ co-ord. (using method of II) | Crest $y$ co-ord. (present method) | Trough $y$ co-ord. (using method of II) | Trough $y$ co-ord. (present method) |
|---|---|---|---|---|---|
| | | | Figure 8 | | |
| 1·0 | 0·5 | 0.415569 | 0·416029 | −0·584523 | −0·583947 |
| 0·8 | 0·3 | 0·236815 | 0·236709 | −0·363180 | −0·363284 |
| 0·6 | 0·1 | 0·074916 | 0·074910 | −0·125082 | −0·125088 |
| | | | Figure 9 | | |
| 0·4 | 0·1 | 0·129693 | 0·129687 | −0·703070 | −0·703370 |
| | | | Figure 10 | | |
| 0·8 | 0·6 | 0·444225 | 0·439341 | −0·757325 | −0·759911 |
| 0·6 | 0·2 | 0·133846 | 0·133782 | −0·265946 | −0·266216 |

TABLE 2. The crest and trough $y$ co-ordinates of waves drawn in figures 8–10, using both methods of computation. N.B. These co-ordinates are *not* all relative to the same mean level.

| $\kappa$ | $h$ | $c^2$ (equation II (3.7$g$)) | $c^2$ (equation (2.47)) |
|---|---|---|---|
| | | Figure 8 | |
| 1·0 | 0·5 | 1·667592 | 1·666525 |
| 0·8 | 0·3 | 1·636259 | 1·635961 |
| 0·6 | 0·1 | 1·554505 | 1·554499 |
| | | Figure 9 | |
| 0·4 | 0·1 | 1·416989 | 1·416948 |
| | | Figure 10 | |
| 0·8 | 0·6 | 1·161923 | 1·162060 |
| 0·6 | 0·2 | 1·463097 | 1·462779 |

TABLE 3. The square of the phase speed $c$ of waves drawn in figures 8–10, using both methods of computation. N.B. The scaling is such that $g = 1$

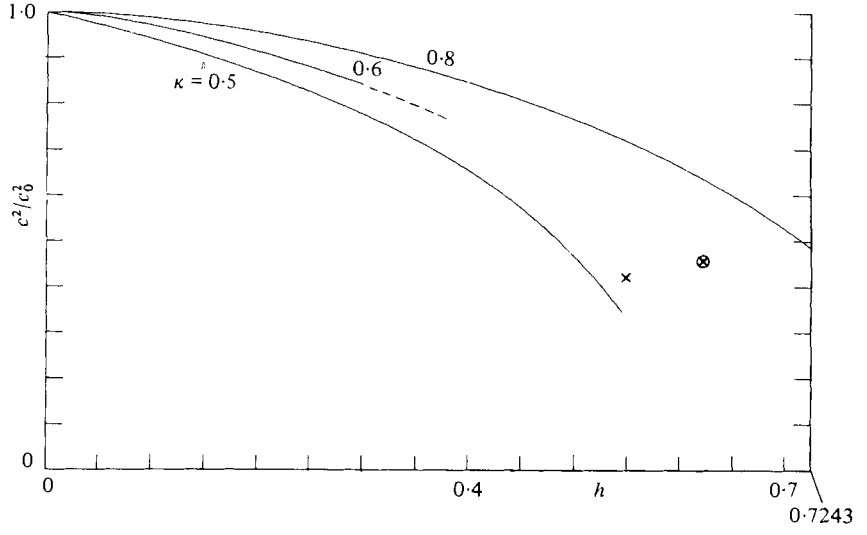


FIGURE 11. The ratio of the squared phase speed, $c^2$, to that of infinitesimal waves, $c_0^2$, plotted against $h$ for $\kappa = 0{\cdot}5$ (capillary-like), 0·6, 0·8. Schwartz & Vanden-Broeck's results for $\kappa = 0{\cdot}5$ (×) and 0·6 (⊗).

now. In table 3, phase speeds are given for the waves drawn in figures 8–10, using the two different methods. The agreement is excellent overall, although the smaller $h/h_{\max}$ and, the nearer $\kappa$ is to $\frac{1}{2}$, the better the agreement. This is also evident in table 2.

Before going on to discuss wave properties in greater detail, it is of interest to find out the results of the perturbation scheme (equation (2.8)), applied as far out as $\kappa = 0{\cdot}3$. This is of course on the far side of another singularity at $\kappa = \frac{1}{3}$ and any agreement must be regarded with scepticism. Nevertheless, some agreement *was* found with the Fourier coefficients $a_n$ and the phase speed $c$. For $\kappa = 0{\cdot}3$ and $h = 0{\cdot}1$, the methods of this paper produced, with $A_1 = -2$, $c^2 = 1{\cdot}325$ and $a_1 = 0{\cdot}0908$.* Using the methods of II, $c^2 = 1{\cdot}325\,18$ and $a_1 = 0{\cdot}090\,85$. Equation (2.8) applied *at* $\kappa = \frac{1}{3}$ was not attempted. A full perturbation scheme based around $\kappa = \frac{1}{3}$ would be preferable, but this has not been undertaken.

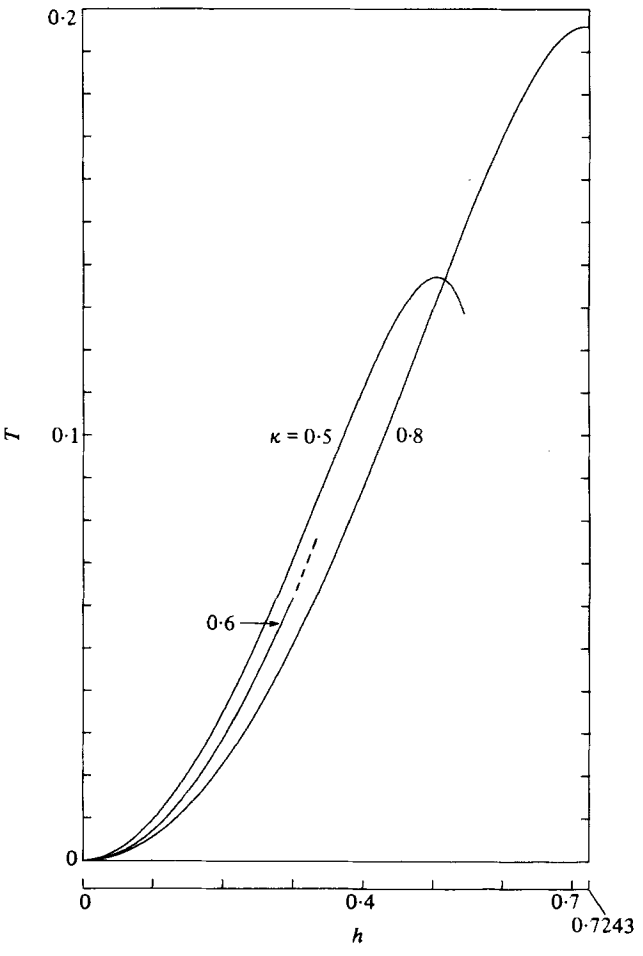


FIGURE 12. The kinetic energy, $T$, plotted against $h$ for $\kappa = 0{\cdot}5$ (capillary-like), 0·6, 0·8. The scaling is such that $\tau = 1$.

### (c) *Wave integral properties*

We now consider integral properties of exact and near-resonance waves, both capillary- and gravity-like, and compare them with values of $\kappa$, dealt with in II and by other authors. So, $\kappa = \frac{1}{2}$ (capillary-like, profiles in figure 4) is compared with $\kappa = 0{\cdot}6$, 0·8 whilst $\kappa = \frac{1}{2}$ (gravity-like, profiles in figure 6) is compared with $\kappa = 0{\cdot}3$, 0·4. The results are given in the appendix. We note that the scaling is always such that $\tau = 1$.

For capillary-like waves, figure 11 shows the ratio $c^2/c_0^2$, where $c_0$ is the phase speed of infinitesimal waves, plotted against the wave semi-height $h$. This immediately reminds us of figure 14 of II, and shows the decrease in phase speed with increasing wave height characteristic of capillary waves. The curve for $\kappa = 0{\cdot}5$ is different in two ways. For small $h$, it moves away from 1 more rapidly than the other curves, owing to the presence of a term in $h$ in $c^2$ (equation 2.42). The rapid rate of decrease of $c^2/c_0^2$ as $h \to h_{\max}$ is probably due to the small number of terms used. Schwartz & Vanden-Broeck's results are included.

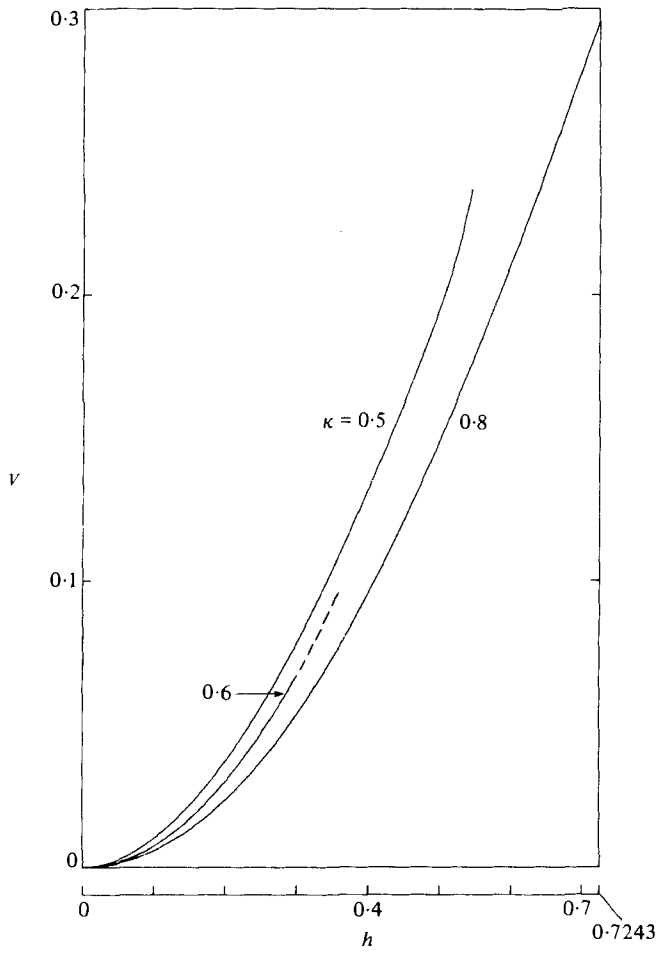


FIGURE 13. The potential energy, $V$, plotted against $h$ for $\kappa = 0{\cdot}5$ (capillary-like), 0·6, 0·8. The scaling is such that $\tau = 1$.

Figure 12 shows the kinetic energy of the capillary-like waves under consideration. A clear maximum is visible for $\kappa = 0{\cdot}5$, far short of $h = h_{\max}$. Such a maximum is also present in the curve $\kappa = 0{\cdot}8$. One would expect a maximum also for $\kappa = 0{\cdot}6$. Figure 13 shows the total potential energy of the same waves. Here we begin to see clear evidence of the special nature of these singular waves. The curve $\kappa = 0{\cdot}5$ has a more rapid increase with $h$ as $h \to h_{\max}$. This special nature is even more evident in figure 14: a graph of the gravitational potential energy $V_g$ versus $h$. In II, figure 17, it is clear that the maximum value of $V_g$ is *reduced* as $\kappa$ decreases from 1, after the initial increase from zero at $\kappa$ infinite. Here this behaviour is confirmed. So much so that the scaled maximum value of $V_g$ for $\kappa = 0{\cdot}5$ is about the same as it is for $\kappa = 5{\cdot}0$. This has a corresponding effect of a greater increase in $V_\tau$, the surface potential energy, which is explained by the dip in the crest of all the waves with $\kappa = 0{\cdot}5$ (capillary-like, figure 4). The last capillary wave integral property at which we will look is the excess flux of $z$ momentum in the $z$ direction, or radiation stress $S_{zz}$: shown in figure 15, corresponding to II, figure 19. Again, we can see the change in trend of values of $S_{zz}$ at the maxima

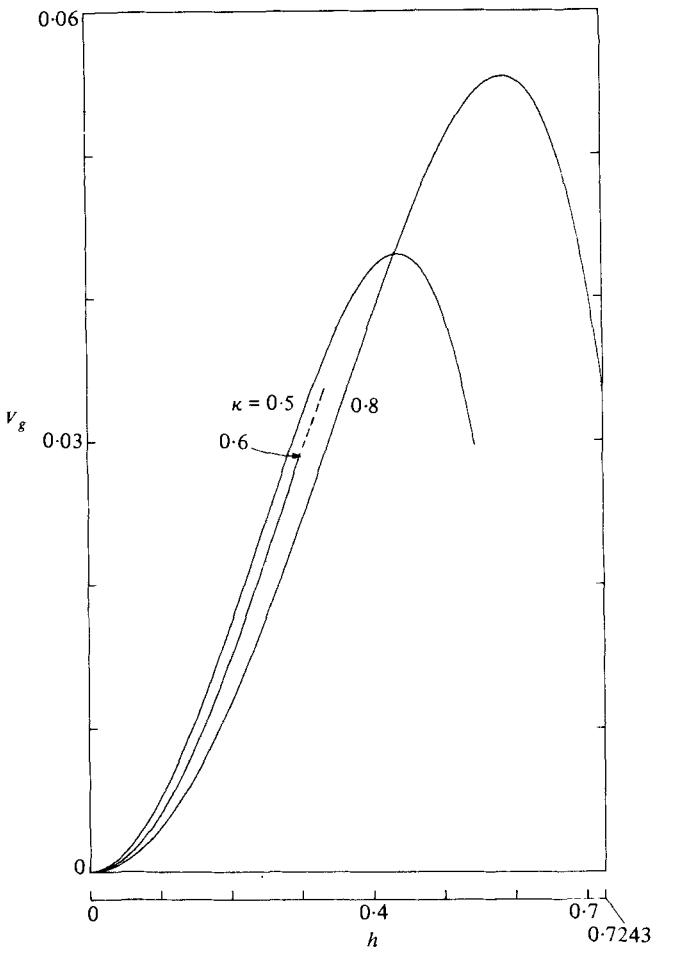


FIGURE 14. That part of the potential energy due to gravity, $V_g$, plotted against $h$ for $\kappa = 0{\cdot}5$ (capillary like), 0·6, 0·8. The scaling is such that $\tau = 1$.

as $\kappa = 0{\cdot}5$ is approached, with $\kappa = 1{\cdot}0$ having approximately the same value as $\kappa = 0{\cdot}5$. And the trend in $\kappa = 0{\cdot}6$ is fairly predictable. Note that $S_{zz}$ is always negative, another characteristic of these capillary waves. The integral properties $I$, $F$ and $S_{xx}$ are not shown because they can easily be obtained from the tables by use of the known formulae given in I. $I$ is given by equation I(2.22), $S_{xx}$ by I(2.23) and $F$ by I(2.24). To find $S_{xx}$, $V_\tau$ must first be calculated. This can be avoided by using equation II(3.18) for $S_{zz}$. For then

$$S_{xx} = 3T - 2V_g + S_{zz} \tag{3.1}$$

or using equation I(2.24)

$$S_{xx} = F/c + S_{zz}, \tag{3.2}$$

and both of these equations use results given in the tables. Even without these results, it is clear that one of the waves at $\kappa = 0{\cdot}5$ is capillary-like in its character, with the highest wave enclosing a bubble of air. All the waves possess properties consistent with capillary waves. It is also evident that there is a smooth transition of wave

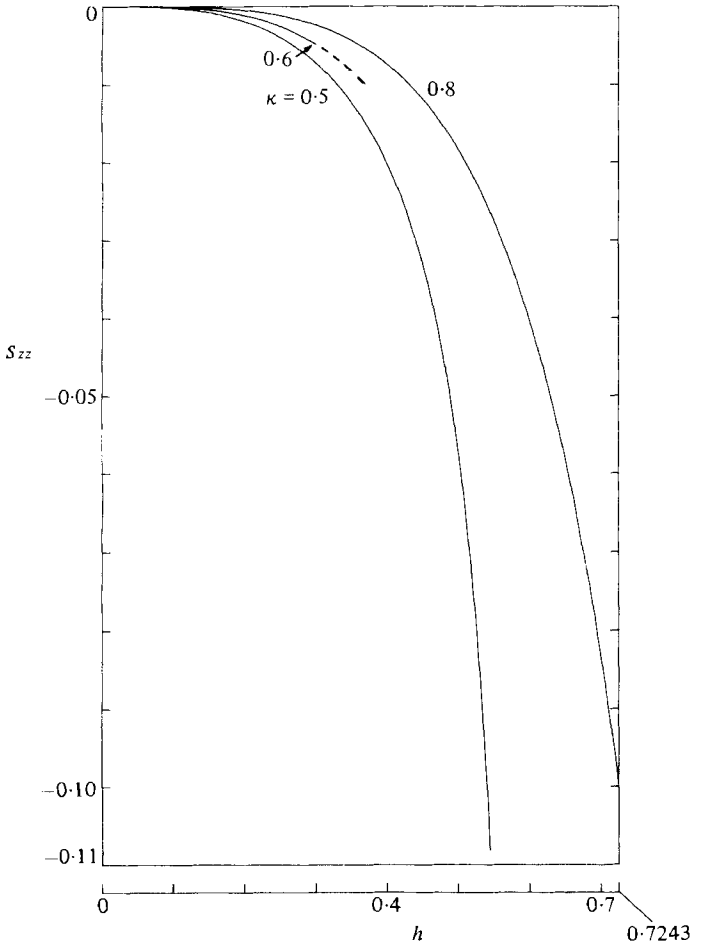


FIGURE 15. The radiation stress, $S_{zz}$, plotted against $h$ for $\kappa = 0{\cdot}5$ (capillary like), 0·6, 0·8. The scaling is such that $\tau = 1$.

properties, as this singularity is approached from shorter wavelengths. The nature of this transition is not, however, monotonic.

Now gravity-like waves: these waves are both capillary- and gravity-like, depending on their height. This is clearly seen in figure 16. Initially the curves of $c^2/c_0^2$ for each value of $\kappa$ increase with $h$, as if they were gravity waves (compare with figure 3 of II). Then, at around $h = 0{\cdot}09$ for $\kappa = 0{\cdot}4$, $h = 0{\cdot}12$ for $\kappa = 0{\cdot}5$, the waves move more slowly as they get higher, thus behaving as capillary waves from then onwards (compare with figure 11 and figure 14 of II). In fact, the highest wave we have shown for $\kappa = 0{\cdot}5$ is slower than even the waves of infinitesimal height. We would expect this trend to continue if we could draw higher waves. The curve for $\kappa = 0{\cdot}3$ shows signs of turning at about $h = 0{\cdot}18$. If this were so, then there exists a definite lag between the appearance of additional troughs and crests in the wave profile, and an overturn in the phase speed curve.

Figures 17 and 18 show the kinetic and potential energies respectively of these gravity-like waves. The curves are remarkably similar at first glance, quite in keeping

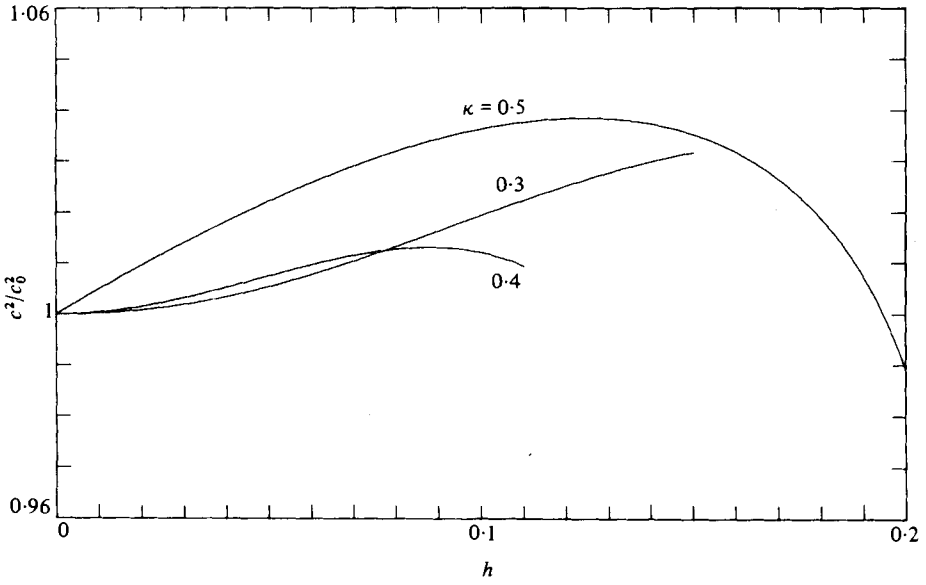


FIGURE 16. The ratio of the squared phase speed, $c^2$, to that of infinitesimal waves, $c_0^2$, plotted against $h$ for $\kappa = 0{\cdot}3$, $0{\cdot}4$, $0{\cdot}5$ (gravity-like).

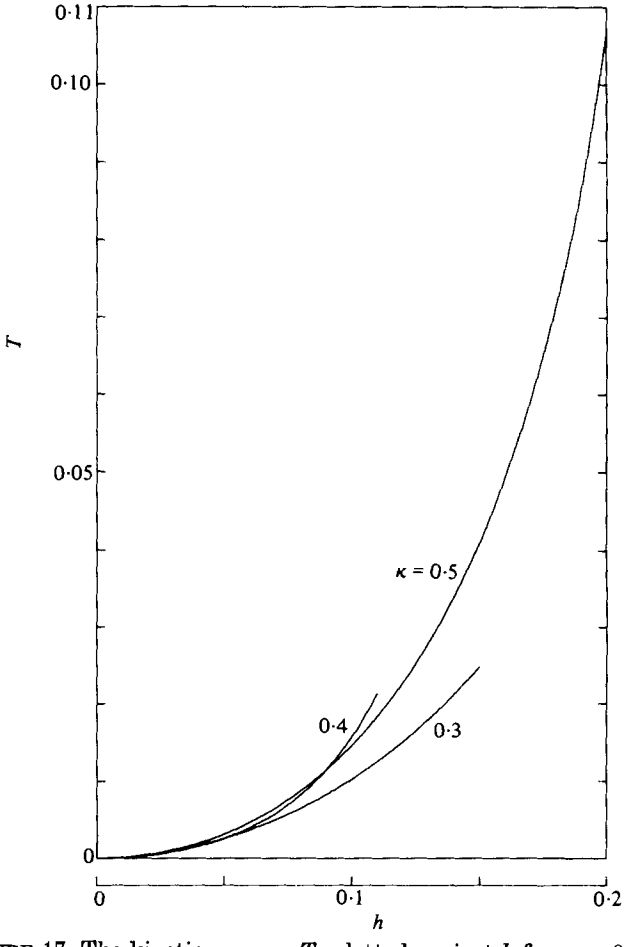


FIGURE 17. The kinetic energy, $T$, plotted against $h$ for $\kappa = 0{\cdot}3$, $0{\cdot}4$, $0{\cdot}5$ (gravity-like). The scaling is such that $\tau = 1$.

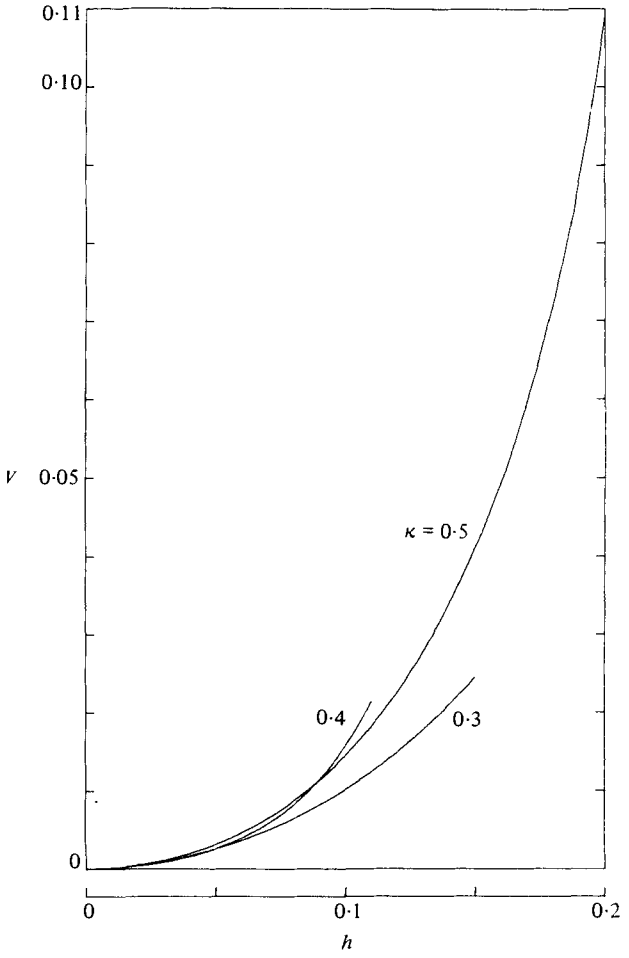


FIGURE 18. The potential energy, $V$, plotted against $h$ for $\kappa = 0{\cdot}3$, $0{\cdot}4$, $0{\cdot}5$ (gravity-like). The scaling is such that $\tau = 1$.

with gravity waves (II, figures 4 and 5) and rather unlike capillary waves (see figures 12 and 13). Of the two waves at $\kappa = 0{\cdot}5$, we can now see that the capillary-like one is less energetic for a given height (by a factor of 3 or so). It is therefore likely to be the more stable one, although no rigorous proof of this is given here. In figure 19 we show the gravitational potential energy. The maxima present in figure 14, and figure 17 of II, are no longer evident, which implies that the waves are no longer totally capillary-like. As the waves become more capillary-like with height, maxima appear (see Schwartz & Vanden-Broeck).

In figure 20, the radiation stress $S_{zz}$ is drawn. The increase with $h$ is characteristic of gravity waves (II, figure 8), whereas the decrease with $h$ is more like the behaviour of capillary waves (II, figure 19). The turning points (possible for $\kappa = 0{\cdot}3$) occur at approximately the same points as for $c^2/c_0^2$ in figure 16.

The non-monotonic variation of the integral properties with $\kappa$ is deceptive. Steady waves of degree 1 are drawn for $\kappa = 0{\cdot}3$ and $0{\cdot}4$; combination (2, 1) waves for $\kappa = 0{\cdot}5$.

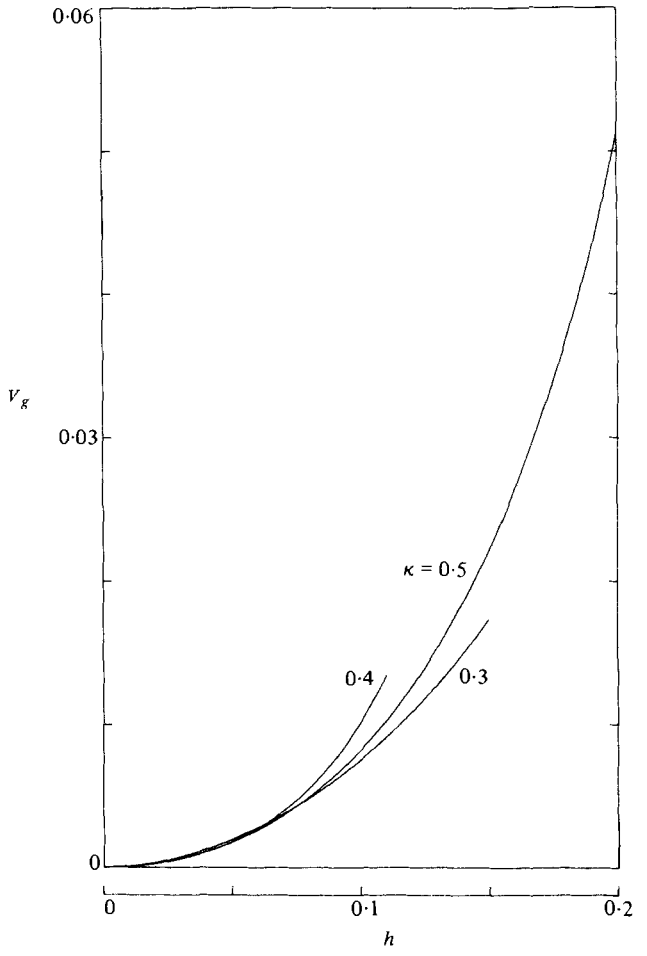


FIGURE 19. That part of the potential energy due to gravity, $V_g$, plotted against $h$ for $\kappa = 0{\cdot}3$, $0{\cdot}4$, $0{\cdot}5$ (gravity-like). The scaling is such that $\tau = 1$.

Overall it is clear that these waves at $\kappa = 0{\cdot}5$ can exhibit both gravity- and capillary-like behaviour depending on their height. There is no great jump in wave properties as this wave is approached from longer wavelengths.

Schwartz & Vanden-Broeck (1979) give results for waves at $\kappa = \frac{1}{2}$ which do not agree with ours for all $h$. Our work has the shortcoming of requiring many more terms than computing facilities would allow. Comparison with their work is difficult owing to lack of tables, but we feel that three-figure accuracy has been obtained up to around $h = 0{\cdot}45$ for capillary-like waves and four figure for $h = 0{\cdot}20$ for gravity-like waves. Convergence was obtained in all cases. Our result for $c$ for capillary-like waves at $h = h_{\max}$ is about 15% smaller. Nevertheless, qualitatively we obtain similar results.

Comparison with the work of Rottman & Olfe (1979) is also qualitatively good, but again no tables are given. We note that figure 2 of that work was given, along with exact analytic results, in an earlier paper by the present author (Hogan 1979*a*).

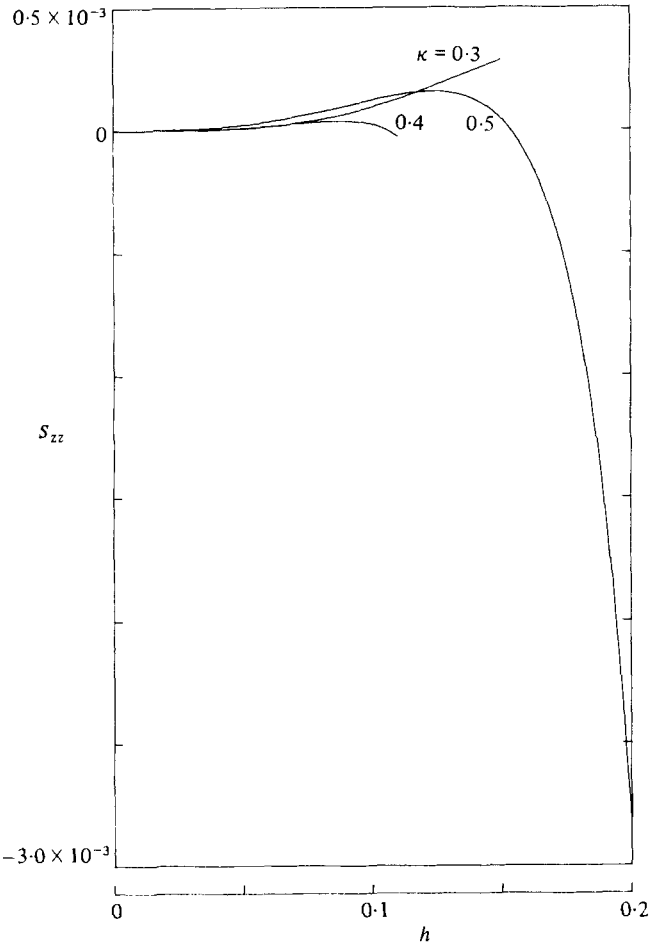


FIGURE 20. The radiation stress, $S_{zz}$, plotted against $h$ for $\kappa = 0{\cdot}3$, $0{\cdot}4$, $0{\cdot}5$ (gravity-like). The scaling is such that $\tau = 1$.

Chen & Saffman (1979) do not give results for waves at or near $\kappa = \frac{1}{2}$. Nayfeh's (1970) equation (4.16*b*) requires a factor of $\alpha k_0$ (his notation) to be added to the right-hand side. His method is a special case of ours, with $A_1 = \alpha\sqrt{2}$, $A_n = 0$ $(n \geqslant 2)$.

To conclude this section we consider properties of gravity-like waves with $\kappa > 0{\cdot}5$ and capillary-like waves with $\kappa < 0{\cdot}5$. We have shown that the wave profile of a particular type does not vary greatly as the singularity is passed from either side. We can therefore expect the same behaviour from the integral properties (not just from one side as we have already shown). In particular, we limit ourselves to the phase speed $c$. In table 4, $c^2$ for capillary-like waves with $\kappa \doteqdot \frac{1}{2}$ is given for five wave heights. Comparison at $h = h_{\max}$ is not useful. Here we can easily see a steady transition *across* the singularity, as indicated in the wave profiles, for a given value of $h$. In table 5 we see the same is true for gravity-like waves, at the four heights we have been able to draw.

In other words, if a capillary-like wave changes its length so as to encounter the first of Wilton's singularities, it need not suffer any great change in character. In fact,

| $h$ | $c^2$ for $A_1 = \frac{1}{100}$ (figure 3) | $c^2$ for $A_1 = 0$ (figure 4) | $c^2$ for $A_1 = -\frac{1}{100}$ (figure 5) |
|---|---|---|---|
| 0·10 | 1·4139 | 1·4123 | 1·4107 |
| 0·20 | 1·3058 | 1·3023 | 1·2988 |
| 0·30 | 1·1711 | 1·1653 | 1·1595 |
| 0·40 | 0·990 | 0·981 | 0·972 |
| 0·50 | 0·72 | 0·70 | 0·69 |

TABLE 4. The square of the phase speed $c$ for capillary-like waves with $\kappa \doteqdot \frac{1}{2}$, as given in figures 3–5. N.B. The scaling is such that $g = 1$.

| $h$ | $c^2$ for $A_1 = \frac{1}{100}$ | $c^2$ for $A_1 = 0$ | $c^2$ for $A_1 = -\frac{1}{100}$ |
|---|---|---|---|
| 0·05 | 1·5339 | 1·5332 | 1·5325 |
| 0·10 | 1·5558 | 1·5544 | 1·5530 |
| 0·15 | 1·5550 | 1·5527 | 1·5505 |
| 0·20 | 1·4889 | 1·4828 | 1·4787 |

TABLE 5. The square of the phase speed $c$ for gravity-like waves with $\kappa \doteqdot \frac{1}{2}$. N.B. The scaling is such that $g = 1$.

it can undergo a smooth transition, still preserving its capillary-like nature. The same is also true for gravity-like waves.

Finally we note that the doubling of wavelength for near-resonance gravity- and capillary-like waves observed by Rottman & Olfe is none other than the bifurcation of waves of degree 2 and length $\lambda$ into combination waves of length $2\lambda$, as given by Chen & Saffman (1979, equation (4.3)).

## 4. Discussion

This paper concludes the present study of steady gravity–capillary waves conducted by the author. Wilton's ripples have been considered in a similar manner to Pierson & Fife (1961). Full agreement has been found with the traditional approach, as given in II. Wave properties are given in graphical and numerical form for some of the waves at $\kappa = \frac{1}{2}$. The other types of wave known to exist at this point can easily be considered by suitable modifications of the basic method. The reason for the appearance of these singularities is the assumption of ordering in the Fourier coefficients, which does not remain consistent throughout the entire gravity–capillary range. This has been summarized in figure 7, clearly illustrating the inability of waves of degree 1 to traverse this range with a non-zero amplitude, as shown by Chen & Saffman.

The limitations of this approach, that is, using Padé approximants, are illustrated in figure 6. No profiles of a highest wave were obtainable for the (2, 1) combination waves at $\kappa = \frac{1}{2}$. This is also true of other work, but the present approach seems more restricted. A computer with more store would be able to produce higher waves. With that reservation, Padé approximants have produced results in agreement with other approaches with a more sound analytical background.

The vast accumulation of theoretical data presented on this subject to date now deserves some experimental attention. The fact that identical conclusions were reached by different methods is not sufficient evidence, in itself, to justify the belief that the real world has been successfully mirrored. A possible experimental procedure, together with some of the expected results, is contained in a brief report by the present author (Hogan 1980*b*). The idea is an old one, based on the fishing-line problem. The theoretical results for the energy flux relative to the 'line' indicate marked changes with increasing amplitude, which may be seen in the laboratory, despite viscous damping, cross currents or other effects.

The solution procedure given in these three parts have been shown to be capable of reproducing results obtained by more sophisticated techniques. In particular there is no inherent drawback in the perturbation scheme we have presented which prevents waves of a given degree from being included. Other combination waves can also be considered. An expansion suitable for combination (3, 1) waves at $\kappa = \frac{1}{3}$ is

$$a_i = \left\{ \begin{array}{ll} \displaystyle\sum_{j=1}^{\infty} \alpha_{ij} \epsilon^{[j+2\mathrm{int}(\frac{1}{4}(i-4))]}, & i \text{ odd}, \\ \displaystyle\sum_{j=1}^{\infty} \alpha_{ij} \epsilon^{[j+2\mathrm{int}(\frac{1}{4}i)+1]}, & i \text{ even}. \end{array} \right\} \tag{4.1}$$

This work does not attempt to be an exhaustive study of the effects of surface tension on steep water waves. With the exception of I, §2, all the results apply to waves on water of infinite depth. The case of uniform finite depth can be considered in a straightforward manner, although the presence of the 'ripple tank' depth should give the problem added interest. At lower depths the dispersion relation is no longer double-valued in the wavenumber and so no 'resonance' is possible. Barakat & Houston (1968) were the first to show that the singular behaviour of the Stokes expansion no longer occurred at these depths. Similarly solitary waves have not been considered.

We have found that great care indeed has to be taken with convergence criteria when using Padé approximants. The series in equations (2.1)–(2.7) converge *very* slowly, even when accelerated. So much so that a limit appears to have been reached when in fact it has not, as highlighted in figure 11.

The case of standing gravity–capillary waves has been considered only by Concus (1962, 1964). There appears to be no simple standing equivalent to Crapper's (1957) solution for pure capillary waves.

I would like to thank Professor M. S. Longuet-Higgins for suggesting this problem to me and the Natural Environment Research Council for financial support while this work was being carried out. This manuscript was prepared when the author was supported by grants from the Office of Naval Research and the Fulbright Scholarship Program of the Council for International Exchange of Scholars at California Institute of Technology, Pasadena.

## Appendix

| $h$ | $c$ | $T$ | $V$ | $V_g$ | $S_{zz}$ |
|---|---|---|---|---|---|
| 0 | 2·0816660 | 0 | 0 | 0 | 0 |
| 0·0225 | 2·0827613 | $0{\cdot}53981\times10^{-3}$ | $0{\cdot}53953\times10^{-3}$ | $0{\cdot}41456\times10^{-3}$ | $0{\cdot}28704\times10^{-6}$ |
| 0·0450 | 2·0861733 | $0{\cdot}20927\times10^{-2}$ | $0{\cdot}20881\times10^{-2}$ | $0{\cdot}15963\times10^{-2}$ | $0{\cdot}46260\times10^{-5}$ |
| 0·0675 | 2·0917358 | $0{\cdot}46153\times10^{-2}$ | $0{\cdot}45929\times10^{-2}$ | $0{\cdot}34752\times10^{-2}$ | $0{\cdot}22407\times10^{-4}$ |
| 0·0900 | 2·0985822 | $0{\cdot}82168\times10^{-2}$ | $0{\cdot}81529\times10^{-2}$ | $0{\cdot}60827\times10^{-2}$ | $0{\cdot}63896\times10^{-4}$ |
| 0·1125 | 2·1055303 | $0{\cdot}13096\times10^{-1}$ | $0{\cdot}12962\times10^{-1}$ | $0{\cdot}95097\times10^{-2}$ | $0{\cdot}13338\times10^{-3}$ |
| 0·1350 | 2·1114469 | $0{\cdot}19497\times10^{-1}$ | $0{\cdot}19274\times10^{-1}$ | $0{\cdot}13848\times10^{-1}$ | $0{\cdot}22326\times10^{-3}$ |
| 0·1425 | 2·1130187 | $0{\cdot}22020\times10^{-1}$ | $0{\cdot}21766\times10^{-1}$ | $0{\cdot}15509\times10^{-1}$ | $0{\cdot}25407\times10^{-3}$ |
| 0·1470 | 2·1138426 | $0{\cdot}23636\times10^{-1}$ | $0{\cdot}23364\times10^{-1}$ | $0{\cdot}16559\times10^{-1}$ | $0{\cdot}27183\times10^{-3}$ |
| 0·1477 | 2·1139707 | $0{\cdot}23913\times10^{-1}$ | $0{\cdot}23638\times10^{-1}$ | $0{\cdot}16738\times10^{-1}$ | $0{\cdot}27471\times10^{-3}$ |
| 0·1485 | 2·1140960 | $0{\cdot}24192\times10^{-1}$ | $0{\cdot}23914\times10^{-1}$ | $0{\cdot}16918\times10^{-1}$ | $0{\cdot}27755\times10^{-3}$ |
| 0·1492 | 2·1142187 | $0{\cdot}24473\times10^{-1}$ | $0{\cdot}24193\times10^{-1}$ | $0{\cdot}17100\times10^{-1}$ | $0{\cdot}28037\times10^{-3}$ |
| 0·1500 | 2·1143385 | $0{\cdot}24757\times10^{-1}$ | $0{\cdot}24474\times10^{-1}$ | $0{\cdot}17282\times10^{-1}$ | $0{\cdot}28316\times10^{-3}$ |

TABLE 6. Properties of the steady wave of degree 1 at $\kappa = 0{\cdot}3$, as a function of the wave semi-height $h$. The scaling is such that $\tau = 1$

| $h$ | $c$ | $T$ | $V$ | $V_g$ | $S_{zz}$ |
|---|---|---|---|---|---|
| 0 | 1·8708287 | 0 | 0 | 0 | 0 |
| 0·0165 | 1·8717895 | $0{\cdot}24288\times10^{-3}$ | $0{\cdot}24276\times10^{-3}$ | $0{\cdot}17292\times10^{-3}$ | $0{\cdot}12260\times10^{-6}$ |
| 0·0330 | 1·8743433 | $0{\cdot}10258\times10^{-2}$ | $0{\cdot}10240\times10^{-2}$ | $0{\cdot}72405\times10^{-3}$ | $0{\cdot}18018\times10^{-5}$ |
| 0·0495 | 1·8777040 | $0{\cdot}25076\times10^{-2}$ | $0{\cdot}24997\times10^{-2}$ | $0{\cdot}17479\times10^{-2}$ | $0{\cdot}79325\times10^{-5}$ |
| 0·0660 | 1·8809161 | $0{\cdot}49711\times10^{-2}$ | $0{\cdot}49509\times10^{-2}$ | $0{\cdot}34081\times10^{-2}$ | $0{\cdot}20233\times10^{-4}$ |
| 0·0825 | 1·8828957 | $0{\cdot}89116\times10^{-2}$ | $0{\cdot}88777\times10^{-2}$ | $0{\cdot}59691\times10^{-2}$ | $0{\cdot}33872\times10^{-4}$ |
| 0·0990 | 1·8822998 | $0{\cdot}15185\times10^{-1}$ | $0{\cdot}15161\times10^{-1}$ | $0{\cdot}98376\times10^{-2}$ | $0{\cdot}24536\times10^{-4}$ |
| 0·1045 | 1·8812521 | $0{\cdot}18008\times10^{-1}$ | $0{\cdot}18002\times10^{-1}$ | $0{\cdot}11506\times10^{-1}$ | $0{\cdot}59717\times10^{-5}$ |
| 0·1078 | 1·8803734 | $0{\cdot}19916\times10^{-1}$ | $0{\cdot}19928\times10^{-1}$ | $0{\cdot}12613\times10^{-1}$ | $-0{\cdot}11763\times10^{-4}$ |
| 0·1083 | 1·8802075 | $0{\cdot}20251\times10^{-1}$ | $0{\cdot}20266\times10^{-1}$ | $0{\cdot}12805\times10^{-1}$ | $-0{\cdot}15306\times10^{-4}$ |
| 0·1089 | 1·8800359 | $0{\cdot}20590\times10^{-1}$ | $0{\cdot}20609\times10^{-1}$ | $0{\cdot}13000\times10^{-1}$ | $-0{\cdot}19033\times10^{-4}$ |
| 0·1094 | 1·8798585 | $0{\cdot}20935\times10^{-1}$ | $0{\cdot}20958\times10^{-1}$ | $0{\cdot}13197\times10^{-1}$ | $-0{\cdot}22950\times10^{-4}$ |
| 0·1100 | 1·8796753 | $0{\cdot}21285\times10^{-1}$ | $0{\cdot}21312\times10^{-1}$ | $0{\cdot}13397\times10^{-1}$ | $-0{\cdot}27064\times10^{-4}$ |

TABLE 7. Properties of the steady wave of degree 1 at $\kappa = 0{\cdot}4$, as a function of the wave semi-height $h$. The scaling is such that $\tau = 1$

| $h$ | $c$ | $T$ | $V$ | $V_g$ | $S_{zz}$ |
|---|---|---|---|---|---|
| 0 | 1·7320508 | 0 | 0 | 0 | 0 |
| 0·0300 | 1·7441584 | $0{\cdot}10752\times10^{-2}$ | $0{\cdot}10705\times10^{-2}$ | $0{\cdot}60292\times10^{-3}$ | $0{\cdot}47188\times10^{-5}$ |
| 0·0600 | 1·7542078 | $0{\cdot}46256\times10^{-2}$ | $0{\cdot}45916\times10^{-2}$ | $0{\cdot}26064\times10^{-2}$ | $0{\cdot}34026\times10^{-4}$ |
| 0·0900 | 1·7615262 | $0{\cdot}11387\times10^{-1}$ | $0{\cdot}11290\times10^{-1}$ | $0{\cdot}64059\times10^{-2}$ | $0{\cdot}96058\times10^{-4}$ |
| 0·1200 | 1·7649359 | $0{\cdot}22654\times10^{-1}$ | $0{\cdot}22499\times10^{-1}$ | $0{\cdot}12603\times10^{-1}$ | $0{\cdot}15451\times10^{-3}$ |
| 0·1500 | 1·7622425 | $0{\cdot}40817\times10^{-1}$ | $0{\cdot}40771\times10^{-1}$ | $0{\cdot}22133\times10^{-1}$ | $0{\cdot}45944\times10^{-4}$ |
| 0·1800 | 1·748236 | $0{\cdot}71070\times10^{-1}$ | $0{\cdot}71868\times10^{-1}$ | $0{\cdot}36622\times10^{-1}$ | $-0{\cdot}79743\times10^{-3}$ |
| 0·1900 | 1·73844 | $0{\cdot}8615\times10^{-1}$ | $0{\cdot}8768\times10^{-1}$ | $0{\cdot}4316\times10^{-1}$ | $-0{\cdot}1531\times10^{-2}$ |
| 0·1960 | 1·7300 | $0{\cdot}974\times10^{-1}$ | $0{\cdot}996\times10^{-1}$ | $0{\cdot}477\times10^{-1}$ | $-0{\cdot}221\times10^{-2}$ |
| 0·1970 | 1·7284 | $0{\cdot}995\times10^{-1}$ | 0·102 | $0{\cdot}486\times10^{-1}$ | $-0{\cdot}234\times10^{-2}$ |
| 0·1980 | 1·7266 | 0·102 | 0·104 | $0{\cdot}494\times10^{-1}$ | $-0{\cdot}249\times10^{-2}$ |
| 0·1990 | 1·7247 | 0·104 | 0·107 | $0{\cdot}503\times10^{-1}$ | $-0{\cdot}265\times10^{-2}$ |
| 0·2000 | 1·7227 | 0·106 | 0·109 | $0{\cdot}512\times10^{-1}$ | $-0{\cdot}281\times10^{-2}$ |

TABLE 8. Properties of the steady combination (2, 1) gravity-like wave at $\kappa = \frac{1}{2}$, as a function of the wave semi-height $h$. The scaling is such that $\tau = 1$

| $h$ | $c$ | $T$ | $V$ | $V_g$ | $S_{zz}$ |
|---|---|---|---|---|---|
| 0 | 1·7320508 | 0 | 0 | 0 | 0 |
| 0·0817 | 1·6911555 | $0{\cdot}66422\times10^{-2}$ | $0{\cdot}67583\times10^{-2}$ | $0{\cdot}35489\times10^{-2}$ | $-0{\cdot}11605\times10^{-3}$ |
| 0·1635 | 1·6401780 | $0{\cdot}24182\times10^{-1}$ | $0{\cdot}25198\times10^{-1}$ | $0{\cdot}12248\times10^{-1}$ | $-0{\cdot}10160\times10^{-2}$ |
| 0·2452 | 1·5776112 | $0{\cdot}50021\times10^{-1}$ | $0{\cdot}53744\times10^{-1}$ | $0{\cdot}23614\times10^{-1}$ | $-0{\cdot}37232\times10^{-2}$ |
| 0·3270 | 1·4977026 | $0{\cdot}81494\times10^{-1}$ | $0{\cdot}91195\times10^{-1}$ | $0{\cdot}34900\times10^{-1}$ | $-0{\cdot}97017\times10^{-2}$ |
| 0·4087 | 1·386733 | 0·11411 | 0·13605 | $0{\cdot}42323\times10^{-1}$ | $-0{\cdot}21934\times10^{-1}$ |
| 0·4905 | 1·212 | 0·1363 | 0·1873 | $0{\cdot}4029\times10^{-1}$ | $-0{\cdot}50951\times10^{-1}$ |
| 0·5177 | 1·126 | 0·1363 | 0·2078 | $0{\cdot}3617\times10^{-1}$ | $-0{\cdot}71448\times10^{-1}$ |
| 0·5450 | 1 | 0·1 | 0·2 | $0{\cdot}3\times10^{-1}$ | −0·1 |

TABLE 9. Properties of the steady combination (2, 1) capillary-like wave at $\kappa = \frac{1}{2}$, as a function of the wave semi-height $h$. The scaling is such that $\tau = 1$

| $h$ | $c$ | $T$ | $V$ | $V_g$ | $S_{zz}$ |
|---|---|---|---|---|---|
| 0 | 1·6329932 | 0 | 0 | 0 | 0 |
| 0·0450 | 1·6273776 | $0{\cdot}13844\times10^{-2}$ | $0{\cdot}13890\times10^{-2}$ | $0{\cdot}84191\times10^{-3}$ | $-0{\cdot}46318\times10^{-5}$ |
| 0·0900 | 1·6134398 | $0{\cdot}57825\times10^{-2}$ | $0{\cdot}57967\times10^{-2}$ | $0{\cdot}33161\times10^{-2}$ | $-0{\cdot}64231\times10^{-4}$ |
| 0·1350 | 1·5946494 | $0{\cdot}13108\times10^{-1}$ | $0{\cdot}13390\times10^{-1}$ | $0{\cdot}72290\times10^{-2}$ | $-0{\cdot}28231\times10^{-3}$ |
| 0·1800 | 1·5724228 | $0{\cdot}23301\times10^{-1}$ | $0{\cdot}24091\times10^{-1}$ | $0{\cdot}12302\times10^{-1}$ | $-0{\cdot}79077\times10^{-3}$ |
| 0·2250 | 1·5471734 | $0{\cdot}36007\times10^{-1}$ | $0{\cdot}37756\times10^{-1}$ | $0{\cdot}18230\times10^{-1}$ | $-0{\cdot}17491\times10^{-2}$ |
| 0·2700 | 1·5188858 | $0{\cdot}50878\times10^{-1}$ | $0{\cdot}54230\times10^{-1}$ | $0{\cdot}24686\times10^{-1}$ | $-0{\cdot}33523\times10^{-2}$ |
| 0·2850 | 1·5087415 | $0{\cdot}56249\times10^{-1}$ | $0{\cdot}60319\times10^{-1}$ | $0{\cdot}26895\times10^{-1}$ | $-0{\cdot}40703\times10^{-2}$ |
| 0·2940 | 1·5024735 | $0{\cdot}59559\times10^{-1}$ | $0{\cdot}64111\times10^{-1}$ | $0{\cdot}28223\times10^{-1}$ | $-0{\cdot}45525\times10^{-2}$ |
| 0·2955 | 1·5014152 | $0{\cdot}60116\times10^{-1}$ | $0{\cdot}64753\times10^{-1}$ | $0{\cdot}28444\times10^{-1}$ | $-0{\cdot}46369\times10^{-2}$ |
| 0·2970 | 1·5003530 | $0{\cdot}60676\times10^{-1}$ | $0{\cdot}65398\times10^{-1}$ | $0{\cdot}28665\times10^{-1}$ | $-0{\cdot}47224\times10^{-2}$ |
| 0·2985 | 1·4992869 | $0{\cdot}61237\times10^{-1}$ | $0{\cdot}66046\times10^{-1}$ | $0{\cdot}28886\times10^{-1}$ | $-0{\cdot}48090\times10^{-2}$ |
| 0·3000 | 1·4982169 | $0{\cdot}61799\times10^{-1}$ | $0{\cdot}66696\times10^{-1}$ | $0{\cdot}29107\times10^{-1}$ | $-0{\cdot}48969\times10^{-2}$ |

TABLE 10. Properties of the steady wave of degree 1 at $\kappa = 0{\cdot}6$ as a function of the wave semi-height $h$. The scaling is such that $\tau = 1$

## REFERENCES


BARAKAT, R. & HOUSTON, A. 1968 *J. Geophys. Res.* **73**, 6545–6555.

CHEN, B. & SAFFMAN, P. G. 1979 *Stud. Appl. Math.* **60**, 183–210.

CHEN, B. & SAFFMAN, P. G. 1980 *Stud. Appl. Math.* **62**, 95–111.

CONCUS, P. 1962 *J. Fluid Mech.* **14**, 568–576.

CONCUS, P. 1964 *J. Fluid Mech.* **19**, 264–266.

CRAPPER, G. D. 1957 *J. Fluid Mech.* **2**, 532–540.

HOGAN, S. J. 1979*a* *J. Fluid Mech.* **91**, 167–180.

HOGAN, S. J. 1979*b* Ph.D. dissertation, University of Cambridge.

HOGAN, S. J. 1980*a* *J. Fluid Mech.* **96**, 417–445.

HOGAN, S. J. 1980*b* Report, California Institute of Technology.

NAYFEH, A. H. 1970 *J. Fluid Mech.* **40**, 671–684.

PIERSON, W. J. & FIFE, P. 1961 *J. Geophys. Res.* **66**, 163–179.

ROTTMAN, J. W. & OLFE, D. B. 1979 *J. Fluid Mech.* **94**, 777–793.

SCHWARTZ, L. W. 1974 *J. Fluid Mech.* **62**, 553–578.

SCHWARTZ, L. W. & VANDEN-BROECK, J.-M. 1979 *J. Fluid Mech.* **95**, 119–139.

WILTON, J. R. 1915 *Phil. Mag.* **29** (6), 688–700.